Assignment, fit, and theoretical discussion of the ν_{10} band of acetaldehyde near 509 cm^{-1}

I. Kleiner [a,*], N. Moazzen-Ahmadi [b], A.R.W. McKellar [c], T.A. Blake [d], R.L. Sams [d], S.W. Sharpe [d], G. Moruzzi [e], J.T. Hougen [f]

[a] Laboratoire Inter-Universitaire des Systèmes Atmosphériques (LISA), CNRS, Université Paris 12 et Paris 7, 61 av Général de Gaulle, 94010 Créteil Cédex, France
[b] Department of Physics and Astronomy, University of Calgary, 2500 University Drive N.W., Calgary, Alberta, Canada T2N 1N4
[c] Steacie Institute for Molecular Sciences, National Research Council of Canada, Ottawa, Ont., Canada K1A OR6
[d] Pacific Northwest National Laboratory, P.O. Box 999, Mail Stop K8-88, Richland, WA 99352, USA
[e] Dipartimento di Fisica dell'Università di Pisa, Largo B. Pontecorvo 3, I-56127 Pisa, Italy
[f] Optical Technology Division, National Institute of Standards and Technology, Gaithersburg, MD 20899-8441, USA

ARTICLE INFO

ABSTRACT

The lowest small-amplitude vibration in acetaldehyde (CH$_3$CHO) is the in-plane aldehyde scissors mode ν_{10} at 509 cm^{-1}. This mode lies about 175 cm^{-1} above the top of the barrier to internal rotation of the methyl group and is relatively well separated from other small-amplitude vibrational states (the next fundamental occurring more than 250 cm^{-1} higher). It thus provides an excellent example of an isolated small-amplitude fundamental (bright state) embedded in a bath of dark states. Since the bath states at these energies are not too dense, and since they arise purely from states of the large-amplitude torsional vibration of the methyl rotor, a detailed spectroscopic analysis of interactions between the bright state and the bath states should be possible. This paper represents the first step toward that goal. We have assigned several thousand transitions in the ν_{10} band ($J \leqslant 28$, $K \leqslant 12$), and have carried out a simultaneous fit of 2400 of these transitions ($J \leqslant 15$, $K \leqslant 9$) with over 8100 transitions to the torsional bath state levels. Three vibration–torsion interactions, which give rise to rather global level shifts of the order of 1 cm^{-1} in the ν_{10} levels, have been identified and quantitatively fit. A number of vibration–torsion–rotation interactions, which give rise to localized (avoided-crossing) shifts in ν_{10} have also been determined. The present analysis indicates the need for reliable spectroscopic information on more of the torsional bath states in the immediate vicinity of the ν_{10} levels. Possible ways of obtaining such information in future studies are considered.

© 2008 Elsevier Inc. All rights reserved.

1. Introduction

The ν_{10} in-plane aldehyde scissors mode at 509 cm^{-1} is the lowest small-amplitude fundamental band of CH$_3$CHO. This mode provides a good example of an isolated small-amplitude fundamental (bright state) embedded in a pure torsional bath (largely dark in absorption from the vibration-torsion ground state). Indeed ν_{10} is relatively well separated from other small amplitude vibrational states (the next higher fundamental occurring more than 250 cm^{-1} higher). Also, the $\nu_{10} = 1$ state lies near the internal rotation $\nu_t = 4$ energy level (about 175 cm^{-1} above the top of the torsional barrier when the torsional zero-point energy of 75 cm^{-1} is accounted for) and so the perturbing levels could be relatively easily identified. This paper represents the first step in an attempt to understand in spectroscopic detail the interaction between this bright state and its surrounding bath.

The paper is divided into three main parts. In the first part (Sections 2–4), we present a traditional spectroscopic analysis and global least-squares fit of more than 10 500 infrared and microwave transitions with $J \leqslant 15$, involving ν_{10} and torsional bath states. In the second part (Section 5), we discuss qualitatively the level of understanding and the many questions resulting from the numerical fits. In the third part (Section 6), we outline directions for future spectroscopic studies to either confirm our present interpretations or to gain additional understanding.

Discussion in all parts will focus separately on three topics: properties of the isolated (in zeroth order) large-amplitude torsional bath, properties of the isolated (in zeroth order) small-amplitude fundamental, and interactions between them. This way of thinking is illustrated by Fig. 1, which shows the three small-amplitude vibrational fundamentals of acetaldehyde below 1000 cm^{-1} on the left and pure torsional states in the same energy region on the right.

The $\nu_t \leqslant 4$ torsional bath states, lying at energies below 600 cm^{-1} on the right of Fig. 1, have been studied in series of papers, as de-
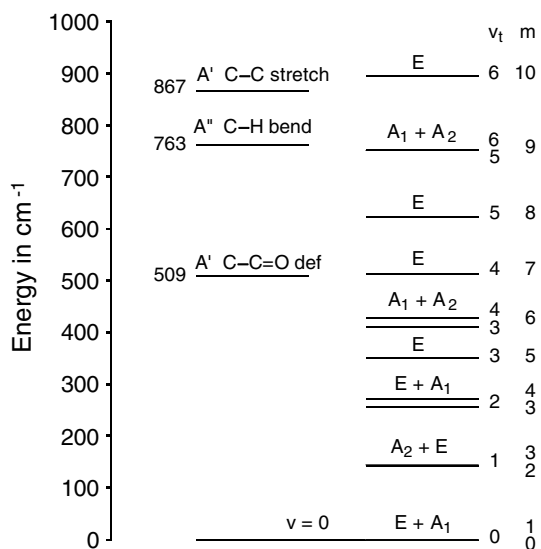
Fig. 1. Low-lying vibrational and torsional levels of acetaldehyde. Energy is plotted in cm^{-1} along the ordinate, with the zero of energy at the ground vibrational level; the minimum of the torsional potential thus lies at approximately -75 cm^{-1} in this figure. The left column shows the lowest three small-amplitude vibrations. The right column shows the lowest torsional levels, which are labeled by the vibrational quantum number v_t (good below the barrier) and by the free-rotor quantum number m (good above the barrier). The present work considers only interactions within the torsional bath, and between the torsional bath and the v_{10} fundamental at 509 cm^{-1}.

scribed in [1] and earlier references cited there. In this work, we extend far-infrared torsional assignments to several hundred transitions in the $v_t = 2 \leftarrow 0$, $3 \leftarrow 1$, and $4 \leftarrow 2$ bands. This extension confirms and somewhat enlarges our previous picture of these torsional bath levels, but as described below, our knowledge of the strongly perturbed $v_t = 4$ torsional manifold is still very incomplete.

The analysis of the v_{10} fundamental carried out here was somewhat challenging because of spectral congestion, line-blending, and perturbations approaching 1 cm^{-1} caused by interactions with the bath. Nevertheless, with the help of a complete Fourier transform spectrum at 195 K, a jet-cooled diode laser spectrum of the band center region, and an automated computer assignment program designed to find branches based on ground state combination differences, we were able to assign about 3500 lines of A and E torsional symmetry species in the v_{10} band with $J \leqslant 28$. A-species subbands cover the range $0 \leqslant K \leqslant 12$. E-species subbands could be identified only for $2 \leqslant |K| \leqslant 12$.

The main difficulty in obtaining an acceptable global fit of the assigned transitions lies in finding which of the many higher-order terms in the Hamiltonian are most appropriate for describing the observed interactions between the small-amplitude fundamental and the torsional bath. In this work we have used group theory and time-reversal to suggest a number of allowed low-order interaction terms, and then selected a suitable set from these by examining energy level diagrams for possible close-lying interaction partners. It appears that the large number of interactions between the bright state and the bath (satisfying a variety of ΔK selection rules in this asymmetric-top molecule) cannot be explained by one or two dominant interaction terms. Our inability to determine a relatively large number of interaction parameters of comparable magnitude from the data set presently available is probably the cause of the fact that the root-mean square of observed-minus-calculated residuals for the v_{10} band from our best least-squares fits is still approximately 18 times experimental measurement uncertainty.

In this connection, it should be noted that a number of studies of small-amplitude vibrations embedded in the torsional bath of

symmetric-top molecules have appeared in the literature, i.e., in CH$_3$CD$_3$ [2], CH$_3$CF$_3$ [3], CH$_3$SiH$_3$ [4], CH$_3$SiD$_3$ [5], CH$_3$CH$_3$ [6], and references cited therein. These studies have achieved least-squares fits of significantly better quality than that achieved here for CH$_3$CHO. We believe there are three main reasons for this. (i) In these CH$_3$XY$_3$ molecules the direction of the methyl top axis coincides with the direction of the symmetric top axis, so there is no competition between internal rotation and overall rotation for the choice of direction of the K-quantization axis (z axis). (ii) CH$_3$XY$_3$ molecules are symmetric tops by symmetry, so the vibration–rotation forces trying to destroy the goodness of the quantum number K for these molecules are much smaller than the rotational forces trying to destroy K in an asymmetric-top like CH$_3$CHO. (iii) CH$_3$XY$_3$ molecules have permutation–inversion groups (i.e., G$_{18}$ when XY$_3 \neq$ CH$_3$ and G$_{36}$ when XY$_3 =$ CH$_3$) which are significantly larger than the G$_6$ group appropriate for CH$_3$CHO. This leads to stricter selection rules for allowed perturbations, and hence to fewer perturbations. Refs. [2–6] make clear, however, that excellent least-squares fits of small-amplitude vibrations embedded in a torsional bath are possible with the proper Hamiltonian.

2. Experimental

Because the present work involves a global fit of extensive data sets obtained in a number of different laboratories by a number of different techniques, the question of absolute calibration for these various data sets arises. We have arbitrarily chosen to convert all later wavenumber measurements to an absolute scale consistent with our earlier published wavenumbers [1], primarily to avoid any confusion that could arise if the absolute wavenumber scale varied from paper to paper in this acetaldehyde series. (Frequency measurements have not been adjusted, of course.) The conversion procedures differ for the two new data sets, as described below.

2.1. NRCC measurements

Two sets of the new measurements treated here were carried out with the modified Bomem [7] instrument at NRCC Ottawa [2], using the same 2 meter cell and the same nominal temperature of 195 K. The first set concerned the v_{10} band and was recorded in 1995. The v_{10} spectrum finally used was recorded at a pressure of 0.07 Torr (1 Torr = 133.3 Pa) and a path length of 48 m (24 traversals of the 2 m cell), in the range from 440 to 590 cm^{-1}. The spectrometer was operated at full resolution (0.0024 cm^{-1} nominal apodized or 0.0018 cm^{-1} unapodized). There was no absolute calibration of the raw spectrum (essentially because the water lines normally used for calibration purposes were absent at 195 K). The second set of measurements concerned the torsional hot bands and was recorded a year later. For these longer wavelength measurements, the spectrometer was operated at a resolution of 0.003 cm^{-1} (nominal apodized), which gives an unapodized instrumental width of about 0.002 cm^{-1}. The path length was 56 m. The spectrum was recorded in three parts, one in the range of 160–230 cm^{-1} at a sample pressure of 0.27 Torr. The other two were at lower frequencies with sample pressures of 0.18 and 0.21 Torr, respectively. Again no absolute calibration was made, so calibration factors were adjusted in the present work to make the new wavenumbers agree with the old [1] wherever the spectra overlapped. In particular, all wavenumbers for the 2–0, 3–1, and 4–2 bands were multiplied by the factor 1.000004660, and all wavenumbers for the new lines in the 3–2 band were multiplied by 1.000007545. (This added from 0.0005 to 0.0008 cm^{-1} to lines in the new spectra.) Measurements from the old and new spectra now agree to within our stated measurement uncertainty for strong lines of 0.00035 cm^{-1} ($v_t =$ 1–0 band) or 0.00050 cm^{-1} (all other torsional bands).

2.2. PNNL measurements

The pulsed supersonic expansion and tunable infrared laser systems used to obtain the jet-cooled spectrum in this work have been described in earlier papers, so only those details relevant to this experiment will be discussed [8–12]. Briefly, light from a lead-salt diode laser is mode filtered by a monochromator and then split sequentially by a three-step chopper mirror. One step sends the light to a 294 MHz free spectral range (FSR) vacuum-spaced confocal etalon, which provides a relative wavenumber scale. A second step sends the light to a one-meter cell filled with 2 Torr of carbonyl sulfide. Measurement of the OCS absorptions provides an absolute wavenumber scale. And the third step sends light into a 2.8 meter optical path White cell that is situated in a vacuum chamber. The plane formed by the laser light crossings in the White cell is elevated such that it intersects the centerline of the jet expansion. Light from all three optical channels are recorded using high speed, photoconductive HgCdTe detectors.

The spectra were recorded with a mixture of 5% acetaldehyde in helium. The acetaldehyde was purchased from Aldrich (99.5+% ACS reagent grade) and was freeze-thawed at liquid nitrogen temperature four times to remove air; no further purification was performed. The mixture was prepared and stored in a 4-l stainless steel cylinder. The mixing cylinder and the stainless steel tubing leading to the pulsed valve were passivated with acetaldehyde before use. The helium/acetaldehyde mixture was expanded through a 12 cm × 200 μ pulsed slit nozzle with a backing pressure of about 520 Torr and the nozzle was operated at 2–3 Hz with a gas pulse duration of about 2.5 ms. Background pressure in the expansion chamber was not allowed to exceed 10^{-4} Torr during operation. Control electronics coordinate the opening of the valve with the rotation of the chopper, ramp the diode laser current (diode temperature is locked) and provide triggering of the transient digitizers that record signals from the three optical channels. The signal data is then stored on a computer. For this experiment each recorded spectral "window" was approximately $0.20 \, \text{cm}^{-1}$ in width and divided into 4096 digitized channels. The available diode provided only discontinuous coverage between 504 and 515 cm^{-1}.

Transition frequencies for the reference gas, carbonyl sulfide (ν_2 fundamental and related hot bands), were taken from the atlas of Maki and Wells [13]. The center frequencies of individual carbonyl sulfide rovibrational transitions used as reference frequencies for the jet spectra were determined by fitting a Gaussian to each individual line. To place an absolute frequency scale on the jet spectrum, first the etalon peak centers were determined relative to the channel number. Next, the reference frequencies from carbonyl sulfide were used to calculate an FSR for the etalon trace and then each transition frequency in the jet spectrum was determined by applying a quadratic interpolation between the three closest etalon peaks. This procedure is followed because of the non-linear scanning characteristics of lead-salt diode lasers. Some portions of the spectrum were scanned several times and this allowed for the determination of the reproducibility (precision) of line center frequency measurements; this was found to be about $\pm 0.0003 \, \text{cm}^{-1}$.

An offset of $0.0016 \, \text{cm}^{-1}$ was subtracted from all diode laser wavenumbers to make them consistent with our earlier infrared measurements. In fact, however, the PNNL diode laser wavenumbers were rather carefully calibrated against the OCS transitions in Maki and Wells [13], and these wavenumbers agree well with PNNL Bruker Fourier transform wavenumbers of acetaldehyde in the same region calibrated against water lines. There is thus reason to believe that the unshifted diode laser measurements represent the best absolute wavenumbers at present.

3. Assignments

Further assignments in the far-IR torsional hot band spectra as well as initial assignments of the mid-IR spectrum of the ν_{10} fundamental were carried out at first by using the usual methods of visual branch identification and ground state combination difference checks. It soon became obvious, however, that this procedure could be made significantly faster by using the RITZ program [14–19], which searches for multiple transitions to the same upper state from different lower state levels, making use at first of a data base of known ground state combination differences and later updating that data base from its own assignments. The RITZ program simultaneously checks all combination differences to all assigned states to which transitions are allowed, and displays on the computer monitor the spectral regions where new extrapolated lines are expected. In this way it is not limited by the available line lists. If line overlappings appear in a few regions, they can be disentangled to a reasonable extent by the procedure described in [19]. Since the RITZ program can check for combination differences enormously faster than a human, it is an excellent tool for extending the *J* range and adding related transitions to fragments of previously assigned branches. It is somewhat less successful, however, at finding new branches where human examination had previously failed, particularly in wavenumber regions containing essentially only blended lines.

In any case, our previous assignments in the $\nu_t = 1 \leftarrow 0$, $2 \leftarrow 1$, and $3 \leftarrow 2$ bands of the $\Delta \nu_t = 1$ far-IR torsional spectrum [1] were significantly augmented by the RITZ procedure. In addition, a number of branches in the $\nu_t = 2 \leftarrow 0$, $3 \leftarrow 1$ and $4 \leftarrow 2$ bands of the $\Delta \nu_t = 2$ spectrum were newly assigned by the RITZ program. Because of the weakness, general spectral congestion, and line-blending of these hot bands, as well as the potential for significant perturbations by the ν_{10} fundamental, considerable care was required in making the new $\nu_t = 3 \leftarrow 1$ and $4 \leftarrow 2$ assignments. Nevertheless, (i) the general consistency of lower and upper state combination differences, (ii) the good agreement of the newly assigned lines with calculations using the old constants [1] (see Section 4), and (iii) the fact that these old constants are from a fit including nearly four hundred pure rotational measurements for $\nu_t = 3$ and 4 levels, all suggest that we have a rather self-consistent picture of the torsional bath manifold, particularly for $\nu_t \leqslant 3$.

The low-*K* subbands near the congested band center of the mid-IR ν_{10} band could not be located with any certainty in the 195 K Fourier transform spectrum, a portion of which is shown in the middle panel of Fig. 2, because of too many (rather than too few) possibilities for branch-like line series in this badly blended region. A similar portion of the fully resolved and rather sparse jet-cooled spectrum is shown in the lower panel of Fig. 2. Combination differences from this very cold spectrum could, in principle, have completely removed any ambiguities in branch assignments in the band center, but the discontinuous spectral coverage associated with lead-salt diodes caused many potential combination difference partners to be missing in our spectrum, thus preventing unambiguous assignment confirmation. Nevertheless, the sparse cold spectrum was still invaluable, since it could be used to verify the existence of low-*J*, low-*K* lines extrapolated from the high-*J* lines of low-*K* branches suggested by the RITZ program.

4. Global fit

4.1. Computer program

We divide the Hamiltonian *H* for this system of interacting levels into three parts, namely: a torsion–rotation part H_{tr} for the vibrational ground state, a torsion–rotation part $H_{\nu_{10}}$ for the
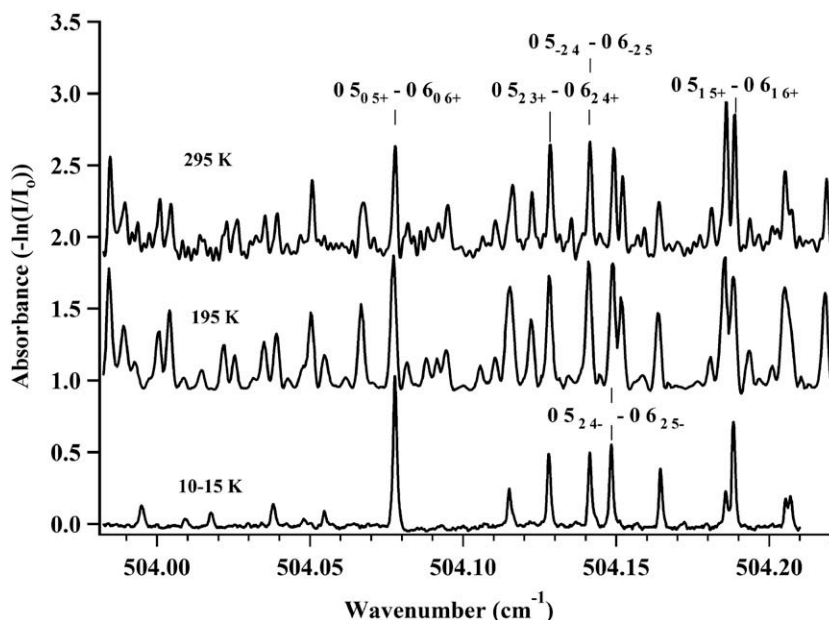
Fig. 2. A portion of the congested center of the ν_{10} band. The upper panel shows a Fourier transform spectrum taken at PNNL at room temperature. The middle panel shows a similar spectrum cooled to 195 K taken at NRCC Ottawa. The lower panel shows a jet-cooled diode laser spectrum taken at PNNL, and illustrates the simplification resulting from the 10–15 K temperature of the sample. Five assigned lines are shown, using the basic notation $v_t' J'_{KaKc} - v_t'' J''_{KaKc}$, where v_t is the torsional quantum number and J_{KaKc} gives the usual asymmetric rotor quantum numbers, but the asymmetric rotor notation has been modified to have a + or − "parity" designation following K_c for A-species levels and a signed value of K_a for E-species levels [1,20].

$\nu_{10} = 1$ fundamental state, and a torsion–rotation part H_{int} describing the interaction between these two systems,

$$H = |v_{10} = 0\rangle\langle v_{10} = 0|H_{tr} + |v_{10} = 1\rangle\langle v_{10} = 1|H_{v_{10}} + [|v_{10}$$
$$= 0\rangle\langle v_{10} = 1| + |v_{10} = 1\rangle\langle v_{10} = 0|]H_{int}, \qquad (1)$$

where the operators H_{tr}, $H_{v_{10}}$, and H_{int} depend only on the torsional angle γ, its conjugate momentum, and the three rotational angular momenta, and where $|v_{10} = 0\rangle$ and $|v_{10} = 1\rangle$ represent the ν_{10} vibrational wavefunctions with $v_{10}=0$ and $v_{10}=1$, respectively. Matrix elements of H are set up using basis functions of the form $|v_{10}\rangle|m\rangle|JK\rangle$, where $|m\rangle = \exp(im\gamma)/\sqrt{2\pi}$ are the usual torsional basis functions and $|JK\rangle$ are the usual $|JKM\rangle$ symmetric-top rotational basis functions for some constant M value (as appropriate in the absence of external fields). The matrix H thus has two large diagonal blocks, one containing the torsion–rotation problem for the ground vibrational state, the other containing an analogous torsion–rotation problem built on ν_{10}. Each of these diagonal blocks is essentially the same as the Hamiltonian matrix described in [1], and will not be described further here.

Matrix elements of H_{int} occur in the off-diagonal blocks connecting these two torsion–rotation problems. Group theory was used to help systematize the search for appropriate interaction terms in H_{int}. Table 1 shows a number of operators from which such interaction terms can be constructed, together with their transformation properties under the G_6 permutation–inversion group appropriate for acetaldehyde [20], as well as under the operation of time-reversal [21]. Products of these operators are allowed in the Hamiltonian if they are Hermitian, belong to the symmetry species A_1 of G_6, and are invariant under time-reversal. We limited our search to operators which contain either one $Q \equiv Q_{10}$ or one $P \equiv P_{10}$, since $\Delta v_{10} = \pm 1$ selection rules must be satisfied when the ν_{10} fundamental interacts with the torsional bath. By further limiting our final selection of interaction operators to those containing only Q_{10} (i.e., not containing P_{10}), we can choose phases of $|v_{10} = 0\rangle$ and $|v_{10} = 1\rangle$ such that all $\Delta v_{10} = \pm 1$ integrals in Q_{10} space yield real and positive matrix elements, which are then conveniently modeled

Table 1
Symmetry properties of various operators[a] used to construct vibration–torsion–rotation perturbation terms[b]

Op[a]	Γ (G_6)[c]	TR[d]	Op[a]	Γ (G_6)[c]	TR[d]
J_x	A_2	−1	Q'	A_1	+1
J_y	A_1	−1	P'	A_1	−1
J_z	A_2	−1	Q''	A_2	+1
$\sin3n\gamma$	A_2	+1	P''	A_2	−1
$\cos3n\gamma$	A_1	+1			
P_γ	A_2	−1			

[a] Operators here are the total angular momentum components (J_x, J_y, J_z), trigonometric functions of the torsional angle γ, the momentum $P\gamma$ conjugate to γ, the small-amplitude vibrational coordinates and conjugate momenta (Q', P') of species A′ in C_s symmetry (including ν_{10} studied here), and their analogs (Q'', P'') of species A″.

[b] Perturbation terms for the vibration–torsion–rotation Hamiltonian are constructed by taking products of operators from this table which are Hermitian, A_1 in G_6, and invariant to time-reversal.

[c] Symmetry Γ of the operator in the group G_6.

[d] Time-reversal (TR) is equivalent to complex conjugation for closed-shell systems [21].

formally in Eq. (1) by the operator $[|v_{10} = 0\rangle\langle v_{10} = 1|+|v_{10} = 1\rangle\langle v_{10} = 0|]$.

The analog of the first-step diagonalization in [1] becomes here a diagonalization of the matrix formed by taking matrix elements of selected $\Delta K = 0$ terms in $|v_{10} = 0\rangle\langle v_{10}=0|H_{tr} + |v_{10} = 1\rangle\langle v_{10} = 1|H_{v_{10}}$ in a $|v_{10}\rangle|m\rangle|JK\rangle$ basis set with $v_{10} = 0$ and 1, and with 21 $m = 0$ mod 3 values for A states in G_6 and 21 $m = 1$ mod 3 values for E states [1]. Since these two matrices are block-diagonal in v_{10} and K, each (v_{10}, K) block is actually diagonalized separately to yield eigenfunctions that can be represented as $|v_{10}\rangle|v_t;K,v_{10}\rangle|JK\rangle$, where: $|v_{10}\rangle$ is taken to be a harmonic-oscillator vibrational wavefunction for the 509 cm^{-1} mode; $|v_t;K,v_{10}\rangle$ is a torsional wavefunction with torsional quantum number v_t; and $|JK\rangle$ is again a symmetric top rotational wavefunction. Note that the torsional eigenfunctions from this first step, $|v_t;K,v_{10}\rangle$, depend somewhat on both K and v_{10}, since they are obtained by diagonalizing separate (v_{10},K) blocks. The var-

ious (v_{10},K) blocks are different, because each block involves torsional parameters depending on v_{10} and a Coriolis interaction depending on K. Because of these differences, the "indices" v_{10} and K must both appear in the torsional eigenfunction labels, and their values must match the quantum numbers v_{10} and K in their harmonic-oscillator and symmetric top partners in the product wavefunction. The second-step diagonalization is then carried out on an A-state or E-state matrix of dimension $2 \times 11 \times (2J + 1)$, which is set up using the 11 lowest-energy $|v_{10}\rangle|v_t;K,v_{10}\rangle|JK\rangle$ torsional eigenfunctions in each diagonal (v_{10},K) block from the first step, for all ($2J + 1$) K values allowed for the given J.

4.2. Data set used in the global fit

While Fig. 1 is useful, it does not tell the whole story because of the rather different K-dependence of torsion-K-rotation energy levels below the barrier (i.e., in the v_{10} fundamental vibrational state) and above it (e.g., in the $v_t = 3$ and 4 torsional states) [1,22]. Thus, for the purpose of understanding the discussion below of energy levels included in, or excluded from, the global fit, we show in Fig. 3 (over a more limited energy region than in Fig. 1) the estimated positions of (hypothetical zeroth order) torsion-K-rotation levels from the small-amplitude vibration v_{10} and from the torsional bath. These energy level positions are actually
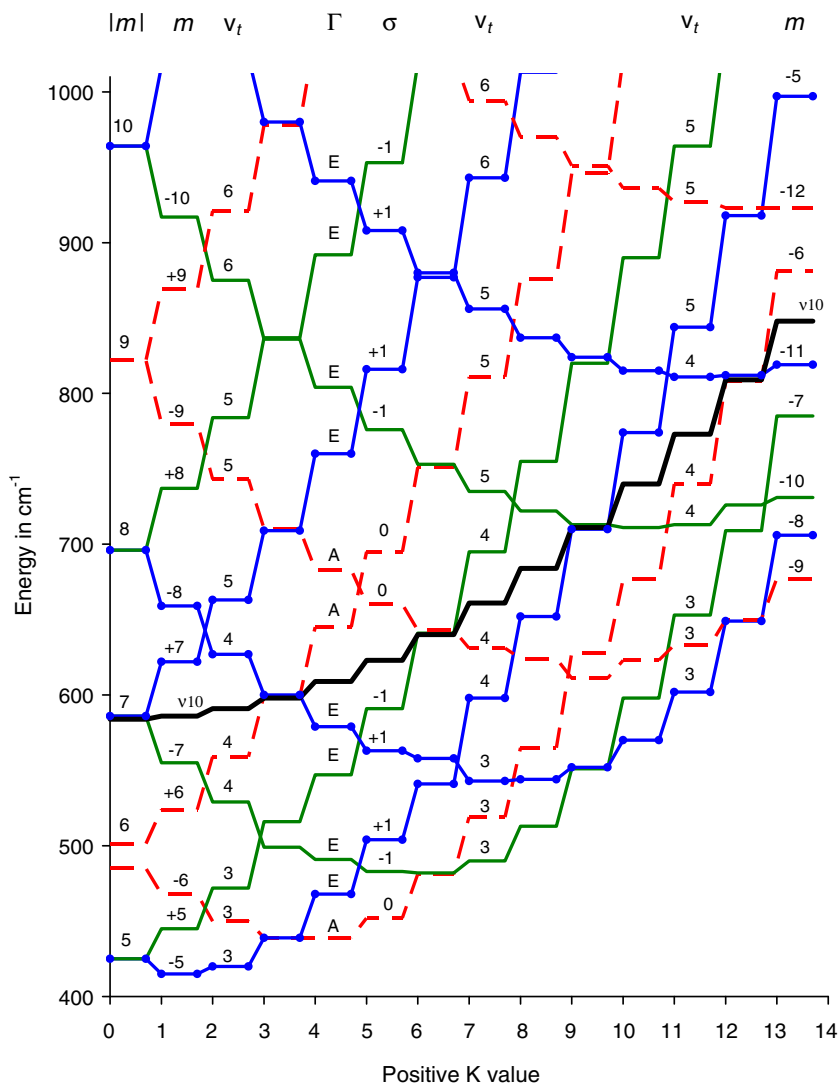
Fig. 3. Low-K torsion-K-rotation levels for the v_{10} fundamental (heavy black line) and for nearby torsional bath states (solid blue, solid green, and dashed red lines), as calculated from Eq. (1) of [1] using constants from the present fit. Energy is plotted in cm^{-1} along the ordinate, with the zero of energy at the bottom of the torsional well; the ground vibrational level thus lies at about +75 cm^{-1} in this figure. Each K value along the abscissa is the K quantum number for all levels in the stack above it. All bath state levels shown lie above the barrier at 407 cm^{-1}. Bath state levels in the stack corresponding to $K = 0$ are labeled by the absolute value of their free-rotor m quantum number. Levels with $m = 0$ mod 3 (dashed red lines) are of A-species in G_6 and levels with $m \neq 0$ mod 3 (solid blue and green lines) are of E-species, as shown by the labels in the $K = 4$ stack. Levels going up in energy from $K = 0$ are $m > 0$ levels; they have the same sign for m and K. Levels going down from $K = 0$ and then going up at some higher K are $m < 0$ levels; they have the opposite sign for m and K. These signed m labels are shown in the $K = 1$ and $K = 13$ stacks. Note that the lines connecting the E-species levels of given $|m|$ or connecting the $|m| = 9$ A-species levels in this figure would be approximately parabolic in shape if all $m < 0$ levels were plotted to the left of the y axis. (See also Figs. 1–4 of [1].) A- and E-species levels can be further characterized by their value of $\sigma \equiv m$ mod 3 for $K > 0$. Blue lines have a value for this quantity of +1, green lines have a value of −1, and red lines have a value of 0, as shown in the $K = 5$ stack. Torsional splittings in the v_{10} levels (labeled in the $K = 1$ and $K = 13$ stacks) are not visible on the scale of this figure, so the heavy black line beginning at 584 cm^{-1} contains the $\sigma = 0$ A levels and the $\sigma = \pm 1$ E levels of v_{10}. The strongest $\Delta K = 0$ interactions between the v_{10} and torsional bath states are expected at the near energy coincidences which occur at $K = 3$, 6, and 12 for A-species levels, and at $\sigma K = 0$, +3, −6, ±9, and +12 for E-species levels. Since K does not change for these interactions, the value of σ must also not change, i.e., only lines of the same color can exhibit $\Delta K = 0$ interactions. As a final point, bath state levels are labeled in the $K = 2$, 7, and 11 stacks by the $v_t = 3$, 4, 5 and 6 quantum numbers used in the fitting program of this paper. Note that each v_t value contains one red, one blue and one green level, and that v_t labels increase monotonically (i.e., {3,3,3}, {4,4,4}, {5,5,5}, etc.) with increasing energy at every K value. (For interpretation of the references to color in this figure legend, the reader is referred to the web version of this paper.)

based on calculations from our fits, but many of the bath levels shown represent extrapolations beyond our fitted data coverage, and their energies must thus be treated as estimated values. Fig. 3 has been designed to highlight the occurrence of nearly degenerate $\Delta K = 0$ (i.e., Fermi-type anharmonic) resonances, because these are expected to be the largest, but a large number of $\Delta K \neq 0$ resonant interactions (avoided crossings) are also observed in the spectrum. Fig. 3 shows that torsion-K-rotation levels of the ν_{10} fundamental move in and out of close $\Delta K = 0$ resonances with various torsion-K-rotation levels of the torsional bath. The bath levels in Fig. 3, which all lie above the torsional barrier, are connected together in a way that shows their relation to the free-rotor m quantum number (just as in Fig. 3 of [1]), since this way of connecting levels will be useful when considering Fig. 4 below. On the other hand, levels in our fitting program and in most of the discussion of this paper are labeled by their ν_t

quantum number. The reader is referred to Fig. 4 of [1] for a diagram with connections drawn to illustrate the ν_t quantum number. The levels in Fig. 3 of the present paper can be connected in this way by turning all crossings between pairs of lines of the same color, i.e., between pairs of dashed red lines (A-species), pairs of solid blue lines with circles (E-species), or pairs of solid green lines without circles (E-species), into avoided crossings. In ν_t language, we would say that the $\nu_t = 3$ A and E levels lie 100 cm^{-1} or more below their $\Delta K = 0$ partner levels in the ν_{10} fundamental, so that the $\nu_t = 3$ levels are not expected to suffer large local perturbations. It is in fact the $\nu_t = 4$ torsional bath levels that move in and out of resonance with ν_{10} as a function of K. Fig. 3 indicates that ν_{10} and $\nu_t = 4$ levels with K equal to a multiple of 3 are most nearly resonant. In particular, A levels with $K = 3$, 6, 12 and E levels with $\sigma K = 0$, +3, −6, ±9, +12 should be most strongly perturbed by $\Delta K = 0$ interactions.
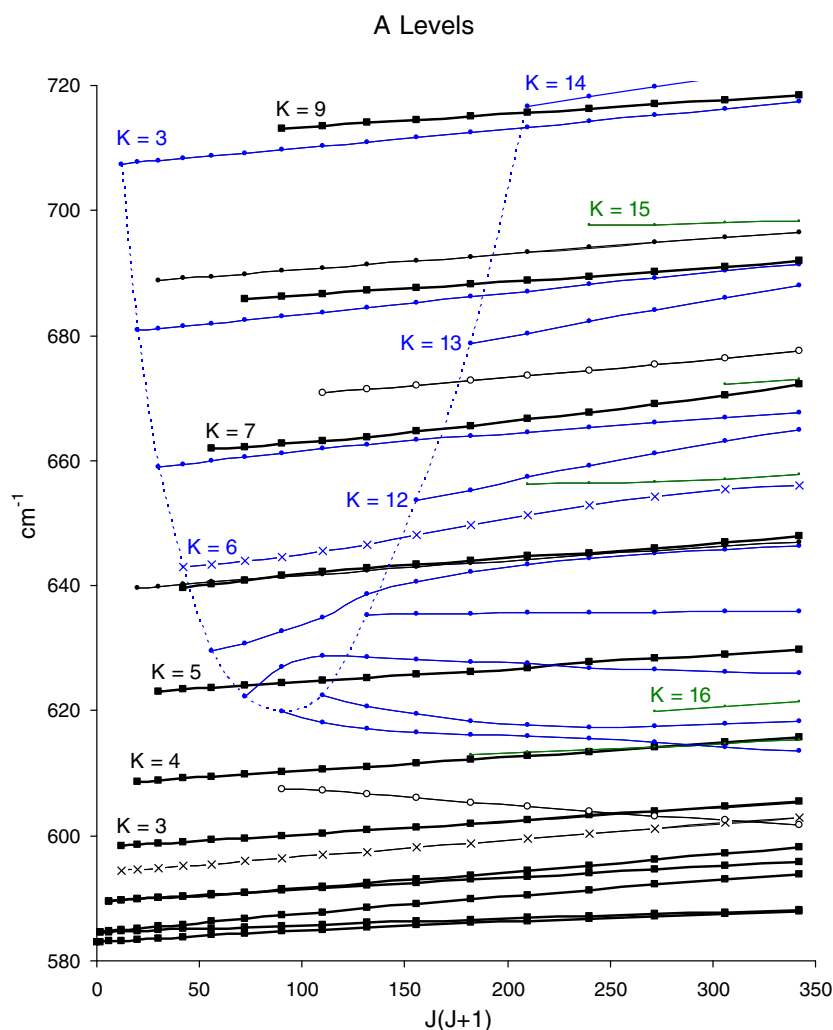

Fig. 4. A-species torsion–rotation energy levels of acetaldehyde in the wavenumber range of 580–720 cm^{-1}, calculated from our global fitting parameters and plotted in the reduced form $E - 0.3J(J + 1)$ against $J(J + 1)$ so that the slopes of curves connecting various series of points with increasing J (J-series) appear as nearly straight, nearly horizontal lines. (i) Energy levels of the ν_{10} fundamental state ($0 \leqslant K \leqslant 9$) are plotted as squares connected by heavy black lines. Only the J-series with $K = 3$, 4, 5, 7, and 9 are labeled, to avoid clutter. Energy positions of the ν_{10} J-series increase approximately as K^2, where K is determined from $K = J$ for the first level in each series. K-type doubling is evident for $K = 1$ and 2 levels. (ii) Bath energy levels with $\nu_t = 1$ ($K = 16$, 17) and $\nu_t = 2$ ($K = 13$, 14, 15) belong to torsional states below the barrier. They are plotted as small circles connected by green lines and interact only slightly with the other levels in the figure. Only the $\nu_t = 1$, $K = 16$ and $\nu_t = 2$, $K = 15$ series are labeled. (iii) Bath energy levels belonging to torsional states above the barrier fall approximately on parabolas [1,22], as illustrated by the dashed blue curve connecting the first point of the solid blue lines with circles. These blue lines form a set of J-series with $3 \leqslant K \leqslant 14$, but only the J-series with $K = 3$, 6, 12, 13, and 14 are labeled. The dashed blue parabola in this figure corresponds to the $|m| = 9$ levels in Fig. 3. (iv) Two J-series from $\nu_t = 4$, one from the blue parabola with $K = 6$ and one with $K = 3$, are plotted as ×'s connected by a solid line. These levels interact rather strongly with $K = 3$ and 6 ν_{10} levels via terms in the Hamiltonian satisfying $\Delta K = 0$ selection rules. (v) The unlabeled J-series plotted as open circles correspond to $\nu_t = 3$, $K = 9$ and $\nu_t = 4$, $K = 10$ in the notation of the fitting program. They represent the only bath state levels in this figure that are experimentally known. (For interpretation of the references to color in this figure legend, the reader is referred to the web version of this paper.)

The present analysis focuses on the interaction of the ν_{10} fundamental with the torsional bath. For that reason, we have excluded from the fit transitions involving torsionally excited levels built on ν_{10}, i.e., transitions involving J and K levels of $\nu_{10} + n\nu_{15}$ with $n > 0$. To avoid considering levels potentially perturbed by this "second" torsional bath, we also imposed an energy cutoff on the fit at the $J = K = 0$ level of $\nu_{10} + \nu_{15}$ by including only reduced energy levels with values of $E - 0.3J(J+1) \leqslant 720 \text{ cm}^{-1}$. This energy cutoff corresponds roughly to the following cutoffs on K values: for ν_{10}, $|K| \leqslant 9$; for $v_t = 4$, $|K| \leqslant 10$; for $v_t = 3$, $|K| \leqslant 13$; for $v_t = 2$, $|K| \leqslant 15$; for $v_t = 1$, $|K| \leqslant 17$; and for $v_t = 0$, $|K| \leqslant 20$.

K values included in the fit were actually somewhat more limited, however. For the ν_{10} fundamental band, $|K| \leqslant 9$ was used as the actual cutoff, with $K' \Gamma' = 0E$, $+1E$, and $-1E$ excluded from the fit because they could not be located with confidence in the dense band center region. For $v_t = 4$, all information used in the present fit comes from the $v_t' \leftarrow v_t'' = 4 \leftarrow 2$ far-infrared band. Since many $v_t = 4$ levels are highly perturbed by interaction with ν_{10}, assignments could not be made with complete certainty, and only fragments of $4 \leftarrow 2$ subbands with $K'\Gamma' = 0A$, $1A$, $10A$, $-4E$, $-3E$, $-2E$, $+5E$, $+6E$, $+7E$ were included in the fit. For this same reason, all of the $v_t = 4-4$ microwave transitions listed in Ref. [1] were also excluded from the present fit. For $v_t = 3$, many levels occurred in both the $v_t' \leftarrow v_t'' = 3 \leftarrow 2$ and $3 \leftarrow 1$ bands, and assignments for this torsional level are thought to be quite secure; thus $v_t = 3$ levels (from microwave and infrared transitions) with $|K'|\Gamma' \leqslant 9A$ and $7E$ were included in the fit. For $v_t = 2$, levels with $|K'|\Gamma' \leqslant 12A$ and $10E$ were included. For $v_t = 1$, levels with $|K'|\Gamma' \leqslant 11A$ and $12E$ were included. For $v_t = 0$, levels with $|K'|\Gamma' \leqslant 13A$ and $12E$ were included.

4.3. Parameter set used in the fit

Although a large number of global fits were carried out, involving different choices for interaction operators and maximum J values, no fit to experimental measurement uncertainty of all observed lines below a reasonable J_{max} emerged. We have nevertheless chosen one of these fits to describe in detail below, because it does in fact significantly increase our understanding of the bright state levels, the torsional bath levels, and their mutual interaction, and it also gives us a logical starting point for the planning of future experimental and theoretical work. In the latter sense it can be thought of as a temporary-use Hamiltonian and fit, which together give calculated frequencies for most of the transitions that fall within the profile of the corresponding observed line. The over 10 500 lines in this fit are not presented here, but the complete output file for the fit discussed below is available as described in Appendix A.

We have not reduced all fixed parameters to zero. For torsional levels arising from the vibrational ground state, some parameters needed at high-J have been fixed to values from a fit with $J \leqslant 26$; other parameters were fixed to "arbitrary" values, obtained when these parameters were floated during the course of earlier fits. Some of these fixed parameters were determinable from the present data set, but floating them led to higher correlation and poorer convergence effects without meaningfully decreasing the overall standard deviation of the fit. Since a new data set (see Section 6) may allow optimum values for many of these parameters to be determined, we decided to simply leave them at fixed values in the present work. For the ν_{10} state, the final choice of the best uncorrelated parameter set is closely connected to the problem of choosing an appropriate reduced Hamiltonian operator (including H_{int} in Eq. (1)), a question which has not yet been considered for this very large system of interacting levels.

Initial guesses for parameters for the torsional bath states, i.e., for torsion–rotation states built on the small-amplitude vibrational ground state were taken from our earlier work [1]. In the fit presented here, 31 ground state parameters were floated and 27 ground state parameters were held fixed, as shown in Tables 2 and 3. Parameters for rotational levels of ν_{10} with no torsional excitation can also be divided into 9 floated and 4 fixed parameters. As can be seen from Table 2, the 4 fixed parameters include 2 parameters describing torsional kinetic and potential energy operators, which cannot be determined without including more torsional states built on ν_{10}. Similarly, interactions between ν_{10} and the torsional bath are described by 8 floated (including the band center = TERM) and 1 fixed parameters. These interaction parameters are given in Table 4. Some of the parameters from the fit will be discussed in more detail in Section 5.

4.4. Quality of the $J \leqslant 15$ global fit

Table 5 gives a summary of the quality of the fit for the various infrared bands and microwave lines from our fit of transitions with $J \leqslant 15$. Looking first at the infrared results, we see that the fits become significantly worse as the maximum value of v_t in the band increases, i.e., as the upper level of the torsional band approaches the energy region of the ν_{10} fundamental. Thus, (i) the $v_t = 1$-0 fundamental band is fit to about 4 times measurement uncertainty, (ii) the $v_t = 2$-1 and 2-0 bands are fit to 3 or 4 times measurement uncertainty, (iii) the $v_t = 3$-2 and 3-1 bands are fit to 8 or 9 times measurement uncertainty, and (iv) the very fragmentary $v_t = 4$-2 band is fit to about 49 times measurement uncertainty. The ν_{10} band itself is fit to about 18 times measurement uncertainty. These infrared results clearly indicate that rotational levels of the $v_t = 0$, 1, and 2 torsional states are fit to an acceptable level of accuracy, but that perturbations between ν_{10} and the close-lying $v_t = 4$ torsional level are not yet fully accounted for. The microwave results are consistent with this, although microwave lines within the various torsional levels are on average fit to only 6–13 times measurement uncertainty, and no $v_t = 4$ - 4 microwave lines were included in the fit because of their very large weighted residuals.

5. Discussion

5.1. Analogy with anharmonic vibrational interaction in the high-barrier case

It is instructive to consider the analog of the present problem in a hypothetical acetaldehyde molecule which does not exhibit internal rotation tunneling splittings, and which therefore belongs to the point group C_s. The interaction between ν_{10} and the $v_t = 4$ torsional level would then be described as an interaction between ν_{10} (A′) and $4\nu_{15}$ (A′). Since these two vibrational states have the same symmetry, the dominant interaction between them would be expected to be anharmonic through a term in the potential energy of the form $Q_{10}Q_{15}^4$. In the present formalism, the small-amplitude vibrational coordinate Q_{10} is retained, but odd powers of the rectilinear torsional coordinate Q_{15}, of species a'' in C_s, must be replaced by some trigonometric function of the internal rotation angle γ of species A_2 in G_6, i.e., by $\sin 3n\gamma$, where n is an integer. Even powers of Q_{15} must be replaced by some trigonometric function of species A_1 in G_6, i.e., by $\cos 3n\gamma$. The term $Q_{10}Q_{15}^4$ must thus be replaced by a term in $Q_{10} \cos 3n\gamma$.

We originally expected that the term with $n = 1$ would explain the bulk of the observed perturbations, reasoning by analogy with the torsional potential function, that the interaction between ν_{10} and the torsional bath would be dominated by the first term in a rapidly convergent Fourier expansion. One can instead, however, reason from the free-rotor limit, characterized by the quantum number m in Fig. 1. The $v_t = 0$ A and E bright states then correspond to $m = 0$ and 1, respectively, while the $v_t = 4$ A and E bath states correspond to $m = 6$ and 7. Such reasoning requires a $\Delta m = 6$ ma-

Table 2
Torsion–rotation parameters with $n = 2$ and 4[a] for the ground ($v_t = 0$, 1, 2, 3 and 4) and ν_{10} ($v_t = 0$) vibrational states of CH_3CHO, from our $J \leqslant 15$ global fit

nlm[a]	Operator[b]	Parameter[b]	($v_t \leqslant 4$ GS)[c] Previous	($v_t \leqslant 3$ GS)[d] Present	$\nu_{10} = 1$[d,e] Present
220	$(1/2)(1 - \cos3\gamma)$	V_3	407.716(10)	408.0791(13)	384.09(32)
	P_γ^2	F	7.5997(28)	7.5597283(73)	7.14085549[g]
211	$P_\gamma P_a$	ρ	0.3316(1)	0.33346543(72)	0.309032(92)
202	P_a^2	A	1.8851594(68)	1.8851373(14)	1.896638(24)
	P_b^2	B	0.3487056(3)	0.34869586(82)	0.349077(19)
	P_c^2	C	0.30318096(4)	0.30317511(25)	0.3027792(60)
	$(P_aP_b + P_bP_a)$	D_{ab}	−0.122636(2)	−0.1226228(49)	−0.12415(11)
440	P_γ^4	k_4	$-0.4384(2) \times 10^{-3}$	$-0.355770321 \times 10^{-3}$[g]	
	$(1/2)(1 - \cos6\gamma)$	V_6	−12.068(37)	−11.93227(65)	−12.067555001[g]
	$\{(1 - \cos3\gamma), P_\gamma^2\}$	k_7	−0.0163(14)	0.00451972180[g]	
431	$P_\gamma^3P_a$	k_3	$-0.8509(3) \times 10^{-3}$	$-0.74820(49) \times 10^{-3}$	
	$\{(1-\cos3\gamma), P_\gamma P_a\}$	k_6	−0.033511565[f]	−0.0336397867[g]	
422	$P_\gamma^2P^2$	G_v	$-0.2966(2) \times 10^{-5}$	$-0.2918(21) \times 10^{-5}$	
	$P_\gamma^2P_a^2$	k_2	$-1.1162(32) \times 10^{-3}$	$-1.07392(50) \times 10^{-3}$	
	$2P_\gamma^2(P_b^2 - P_c^2)$	c_1	$-0.405(4) \times 10^{-5}$	$-0.518(15) \times 10^{-5}$	
	$P_\gamma^2(P_aP_b + P_bP_a)$	Δ_{ab}	$0.401(3) \times 10^{-4}$	$0.4238(34) \times 10^{-4}$	
	$\sin3\gamma(P_aP_c + P_cP_a)$	D_{ac}	$-0.185(4) \times 10^{-2}$	$-0.1459(44) \times 10^{-2}$	
	$\sin3\gamma(P_bP_c + P_cP_b)$	D_{bc}	$-0.341(5) \times 10^{-3}$	$-0.495(18) \times 10^{-3}$	
	$(1 - \cos3\gamma)P^2$	F_v	$0.55891(6) \times 10^{-3}$	$0.57977(66) \times 10^{-3}$	
	$(1 - \cos3\gamma)P_a^2$	k_5	−0.0380(3)	−0.0425010(44)	
	$(1 - \cos3\gamma)(P_b^2 - P_c^2)$	c_2	$0.20878(8) \times 10^{-3}$	$0.21129(46) \times 10^{-3}$	
	$(1 - \cos3\gamma)(P_aP_b + P_bP_a)$	d_{ab}	$0.20996(6) \times 10^{-2}$	$0.21100(36) \times 10^{-2}$	
413	$P_\gamma P_a P^2$	L_v	$0.578(2) \times 10^{-5}$	$0.5695(33) \times 10^{-5}$	
	$P_\gamma P_a^3$	k_1	$-0.6753(1) \times 10^{-3}$	$-0.66188(20) \times 10^{-3}$	
	$P_\gamma\{P_a(P_b^2 - P_c^2)\}$	c_4	$-0.526(3) \times 10^{-5}$	$-0.624(16) \times 10^{-5}$	
	$P_\gamma(P_a^2P_b + P_bP_a^2)$	δ_{ab}	$0.450(4) \times 10^{-4}$	$0.449750473 \times 10^{-4}$[g]	
404	$-P^4$	D_J	$0.3119(1) \times 10^{-6}$	$0.31006(48) \times 10^{-6}$	$0.252(21) \times 10^{-6}$
	$-P^2P_a^2$	D_{JK}	$-0.442(2) \times 10^{-5}$	$-0.4767(45) \times 10^{-5}$	$-0.1972(71) \times 10^{-5}$
	$-P_a^4$	D_K	$0.1518(4) \times 10^{-3}$	$0.150265(94) \times 10^{-3}$	$0.2692(17) \times 10^{-4}$
	$-2P^2(P_b^2 - P_c^2)$	δ_J	$0.7068(5) \times 10^{-7}$	$0.7026(24) \times 10^{-7}$	$0.691460909 \times 10^{-7}$[g]
	$-\{P_a^2(P_b^2 - P_c^2)\}$	δ_K	$0.1306(8) \times 10^{-5}$	$0.1202(39) \times 10^{-5}$	$0.103534182 \times 10^{-5}$[g]
	$(P_aP_b + P_bP_a)P^2$	D_{abJ}	$0.670(2) \times 10^{-6}$	$0.6286(75) \times 10^{-6}$	
	$(P_a^3P_b + P_bP_a^3)$	D_{abK}	$0.103(1) \times 10^{-4}$	$0.837(29) \times 10^{-5}$	

[a] Notation of Ref. [1]: $n = l + m$, where n is the total order of the operator, l is the order of the torsional part and m is the order of the rotational part, respectively.

[b] Notation of Ref. [1]: $\{A,B\} = AB + BA$. The product of the parameter and operator from a given row yields the term actually used in the vibration–rotation–torsion Hamiltonian, except for F, ρ and A, which occur in the Hamiltonian in the form $F(P_\gamma + \rho P_a)^2 + AP_a^2$.

[c] Values of the parameters from an earlier ground state (GS) fit of $v_t \leqslant 4$ [1]. All values are in cm^{-1}, except for ρ which is unitless. Statistical uncertainties are shown as one standard uncertainty ($k = 1$) [23] in the last digit.

[d] Values of the parameters from the present fit, involving torsional states $v_t \leqslant 3$ for the microwave data and $v_t \leqslant 4$ for the far-infrared data. For $\nu_{10} = 1$ only the $v_t = 0$ torsional state data is involved. Units and uncertainties as in footnote c.

[e] Parameters with no value indicated were set to zero.

[f] The parameter k_6 was held fixed in our earlier work on $v_t \leqslant 4$ levels [1].

[g] Values of the parameters kept fixed in the present work (see text).

trix element, and suggests that the $Q_{10} \cos3n\gamma$ term with $n=2$ will dominate any direct interaction, and, further, that interactions via the term with $n = 1$ will be second-order in nature, resulting in strong accompanying perturbations of the lower v_t levels.

In the fit presented here, we simultaneously floated coefficients of the $Q_{10} \cos3n\gamma$ terms with $n = 1$, 2, and 3, which Table 4 indicates are all determined to better than 1%, with the $n = 3$ term largest. This result hints at the theoretically unwelcome conclusion that the bright-state−bath-state interaction under study here may result from a number of perturbations of similar size, a conclusion that is reinforced by noting that the coefficient of $Q_{10} P\gamma^2$ was also floated and determined to better than 1%.

5.2. Reduced rotational energy levels

Fig. 4 shows, in an effort to better understand the complexity of the perturbation problem, the calculated reduced energy positions, $E-0.3J(J + 1)$, of all A-species torsion–rotation levels with $J \leqslant 18$ lying in the energy range from 580 to 720 cm^{-1}, as obtained from our fitting parameters. Calculated level positions are indistinguishable from observed level positions (when they exist) on the scale of Fig. 4. Various series of levels with fixed K and increasing J (called J-series for short) are connected together by solid lines. The K value for each J-series is determined by the

fact that the series starts at $J = K$. Many of the connecting lines are characterized by a small positive slope, indicating that the effective B value for such a J-series is nearly constant and slightly larger than 0.3 cm^{-1}.

The energy range of Fig. 4 includes ν_{10} A-species levels with $0 \leqslant K \leqslant 9$. These are shown as squares connected by thick black lines and are the main focus of this paper. The J-series for ν_{10}, which all involve rotational levels in the torsional ground state of this small-amplitude fundamental, increase in energy approximately as K^2. K-type doubling can be seen clearly only for the $K = 1$ and 2 levels of ν_{10} on the scale of Fig. 4.

The energy range of Fig. 4 also includes over 20 J-series from the torsional bath, none of which, except for the $v_t = 3$, $K = 9$ and $v_t = 4$, $K = 10$ series indicated by the black open circles near 605 and 670 cm^{-1}, respectively, have been located experimentally. Various patterns can be recognized in the bath-state J-series. Some levels in the energy region of Fig. 4 arise from torsional states below the barrier. These are represented by the green lines on the right of the diagram, corresponding to the J-series for $K = 16$ and 17 of $v_t = 1$ and for $K = 13$ (near 610 cm^{-1}), 14, and 15 of $v_t = 2$. Energies for these J-series also increase approximately as K^2. We do not expect rotational levels of these series to interact significantly with the ν_{10} levels, and they will not be discussed further here. Other bath-state rotational levels arise from torsional states above the

Table 3
Torsion–rotation parameters with $n \geqslant 6$[a] for the ground (v_t = 0, 1, 2, 3 and 4) vibrational state of CH_3CHO, from our $J \leqslant 15$ global fit. Parameters with $n \geqslant 6$ were not used for the v_{10} = 1 state

nlm[a]	Operator[b]	Parameter[b]	($v_t \leqslant 4$ GS)[c] Previous	($v_t \leqslant 3$ GS)[d,e] Present
660	$(1/2)(1 - \cos 9\gamma)$	V_9	$-0.186(2)$	0.160753739[g]
	P_γ^6	k_{4B}	$-0.820(4) \times 10^{-6}$	$-0.819877980 \times 10^{-6g}$
651	$P_\gamma^5 P_a$	k_{3B}	$-0.119(1) \times 10^{-5}$	$-0.118723999 \times 10^{-5g}$
642	$(1 - \cos 6\gamma)P^2$	N_v	$0.554(1) \times 10^{-4}$	$0.554231744 \times 10^{-4g}$
	$(1 - \cos 6\gamma)P_a^2$	K_2	$0.395(20) \times 10^{-3}$	$0.395282574 \times 10^{-3g}$
	$P_\gamma^4 P_a^2$	K_1	$-0.56(1) \times 10^{-6}$	$-0.6157(33) \times 10^{-6}$
	$P_\gamma^4 P^2$	M_v	Not used	$0.114(36) \times 10^{-8}$
	$2P_\gamma^4(P_b^2 - P_c^2)\,P_a$	c_3	$0.29(1) \times 10^{-8}$	$0.287599224 \times 10^{-8g}$
	$\{(1 - \cos 3\gamma),\, P_\gamma^2\}\,P_a^2$	k_{7K}	$0.64(2) \times 10^{-4}$	$0.708649437 \times 10^{-4g}$
	$(1 - \cos 6\gamma)(P_a P_b + P_b P_a)$	dd_{ab}	$-0.705(7) \times 10^{-4}$	$-0.704513011 \times 10^{-4g}$
633	$P_\gamma^3 P^2 P_a$	k_{3J}	$-0.59(2) \times 10^{-8}$	$-0.589573082 \times 10^{-8g}$
	$\{(1 - \cos 3\gamma),\, P_\gamma P_a^3\}$	k_{6K}	$0.5677008 \times 10^{-4f}$	0.568×10^{-4g}
624	$P_\gamma^2 P^2 P_a^2$	k_{2J}	$-0.74(1) \times 10^{-8}$	$-0.74224982 \times 10^{-8g}$
	$P_\gamma^2 P_a^4$	k_{2K}	$0.162(3) \times 10^{-6}$	$0.162172792 \times 10^{-6g}$
	$(1 - \cos 3\gamma)(P_b^2 - P_c^2)P^2$	c_{2J}	$-0.44(1) \times 10^{-8}$	$-0.440225596 \times 10^{-8g}$
	$2P_\gamma^2(P_b^2 - P_c^2)\,P^2$	c_{1J}	$0.29(4) \times 10^{-10}$	$0.2895457 \times 10^{-10g}$
	$(1 - \cos 3\gamma)P^4$	f_v	$-0.722(5) \times 10^{-8}$	$-0.722018012 \times 10^{-8g}$
	$(1 - \cos 3\gamma)P_a^4$	f_k	$0.246(3) \times 10^{-4}$	$0.246074639 \times 10^{-4g}$
615	$P_\gamma P_a P^4$	l_v	$0.18(2) \times 10^{-10}$	$0.1833131 \times 10^{-10g}$
	$P_\gamma P_a^5$	l_k	$0.86(1) \times 10^{-7}$	$0.859124140 \times 10^{-7g}$
	$P_\gamma P_a^3 P^2$	λ_v	$-0.544(6) \times 10^{-8}$	$-0.543516266 \times 10^{-8g}$
606	$P_a^4 P^2$	H_{KJ}	$-0.144(1) \times 10^{-8}$	$-0.143862478 \times 10^{-8g}$
	P_a^6	H_K	$0.149(3) \times 10^{-7}$	$0.148832687 \times 10^{-7g}$
880	$(1/2)(1 - \cos 12\gamma)$	V_{12}	$0.1076(2)$	-0.00587328782[g]
1082	$(1 - \cos 12\gamma)P^2$	V_{12J}	$-0.191(4) \times 10^{-5}$	$-0.191054708 \times 10^{-5g}$

[a] Notation of Ref. [1]: $n = l + m$, where n is the total order of the operator, l is the order of the torsional part and m is the order of the rotational part, respectively.
[b] Notation of Ref. [1]: $\{A,B\} = AB + BA$. The product of the parameter and operator from a given row yields the term actually used in the vibration–rotation–torsion Hamiltonian.
[c] Values of the parameters from an earlier ground state (GS) fit of $v_t \leqslant 4$ [1]. All values are in cm^{-1}. Statistical uncertainties are shown as one standard uncertainty ($k = 1$) [23] in the last digit.
[d] Values of the parameters from the present fit, involving torsional states $v_t \leqslant 3$ for the microwave data and $v_t \leqslant 4$ for the far-infrared data. For v_{10} = 1 only the v_t = 0 torsional state data is involved. Units and uncertainties as in footnote c.
[e] Parameters with no value indicated were set to zero.
[f] The parameter k_{6K} was held fixed in our earlier work on $v_t \leqslant 4$ levels [1].
[g] Values of the parameters kept fixed in the present work (see text).

Table 4
Band origin for v_{10} and vibration–torsion–rotation parameters describing interactions between the ground vibrational state (v_t = 0, 1, 2, 3 and 4) of CH_3CHO (bath levels) and the v_{10} = 1 bright state (v_t = 0), from our $J \leqslant 15$ global fit

nlm[a]	Operator[b]	Parameter[b]	Present results[c]
220	$Q_{10}P_\gamma^2$	WF	$-0.12806(20)$
	$Q_{10}(\cos 3\gamma)$	WC3	$5.186(12)$
440	$Q_{10}(\cos 6\gamma)$	WC6	$-11.030(19)$
660	$Q_{10}(\cos 9\gamma)$	WC9	$13.600(14)$
651	$Q_{10}\{\cos 6\gamma, P_\gamma P_a\}$	WFB6	$0.001297(46)$
642	$Q_{10}(\cos 6\gamma)P^2$	WNV	$-0.000897(21)$
	$Q_{10}(\cos 6\gamma)P_a^2$	WBK2	-0.00772507538[d]
862	$Q_{10}(\cos 9\gamma)P_a^2$	WC9 K	$0.004419(73)$
Band origin for v_{10}		TERM	$512.558(34)$

[a] See Tables 2 and 3.
[b] See Tables 2 and 3. Note that all these operators achieve a non-zero v_{10}-bath interaction via the factor Q_{10}. Note also that the traditional ordering scheme is not meaningful for interaction operators in this table, since the operators with nlm = 220, 440, and 660 increase in magnitude.
[c] All values are in cm^{-1}. Statistical uncertainties are one standard uncertainty ($k = 1$) [23] in the last digit.
[d] WBK2 was held fixed at this value during the fit.

barrier. The first levels of such J-series for different K values lie approximately on parabolas [1,22], one of which (corresponding to the $|m| = 9$ levels from Fig. 3) happens to lie in the energy region of Fig. 4, as illustrated by the $J = K$ levels connected by the blue dashed curve on the left of the figure. The J-series for these levels are represented by solid blue lines with circles. Many of these

J-series lines are not straight, and many that are straight are not horizontal, indicating that the series are described by effective B values that are somewhat irregular. As can be seen from Fig. 3, the v_t values for series connected by this parabola are not all the same. In fact, the $K = 3–4$ points on the parabola have $v_t = 5$, the $K = 5–9$ points have $v_t = 4$, and the $K = 10–14$ points have $v_t = 3$.

The levels of two bath-state series in Fig. 4, having $v_t = 4$, $K = 3$ and $v_t = 4$, $K = 6$, respectively, are indicated by the symbol ×. As can be seen from the dashed lines in the torsion-K-rotation energy level overview of Fig. 3, these two J-series of A levels are expected to lie very close in energy to a series of A levels with the same K value in v_{10}. Since we use mainly v_{10}-bath interaction terms satisfying $\Delta K = 0$ selection rules in the present fit (see Table 4), the pair of $K = 3$ levels shown in Fig. 4 as solid squares and ×s and the analogous pair of $K = 6$ levels indicate the main v_{10}-bath interactions for A levels determined in the present work. By examining these two interactions in detail, we find that the $K = 3$ levels of v_{10} near 598 cm^{-1} in Fig. 4 appear to be pushed up by the $K = 3$ bath levels (- × -) near 594 cm^{-1} by almost 1 cm^{-1}. This relatively large perturbation has been successfully included in our fitting Hamiltonian, since the residuals for transitions to the v_{10} $K = 3$ levels are generally smaller than 0.002 cm^{-1}, as shown in Table 6. The $K = 6$ levels of v_{10} near 640 cm^{-1} appear to be perturbed by the $K = 6$ bath levels (- × -) near 643 cm^{-1}. This perturbation is less well accounted for in our fit, since some low-J observed-minus-calculated residuals for transitions to the v_{10} $K = 6$ levels in Table 6 reach 0.015 cm^{-1}.

Table 5
Overview of root-mean-square deviations (RMS) of observed-minus-calculated residuals from the present fit of 10 587 transitions

Type[a]	Number[b]	$v_t' \leftarrow v_t''$	RMS[c]	RMS[d]	Type[e]	Number[b]	Meas. Unc.[f]	RMS[c]	RMS[d] (MHz)
MW	660	$0 \leftarrow 0$	6.1	0.36 MHz	MW	11	4 kHz	29.7	0.12
MW	535	$1 \leftarrow 1$	8.2	0.70 MHz	MW	62	20 kHz	11.0	0.22
MW	351	$2 \leftarrow 2$	11.0	1.05 MHz	MW	487	45 kHz	8.3	0.40
MW	200	$3 \leftarrow 3$	13.4	2.53 MHz	MW	305	70 kHz	15.9	1.12
IR	1403	$1 \leftarrow 0$	3.6	1.3×10^{-3} cm^{-1}	MW	386	80 kHz	4.6	0.37
IR	1146	$2 \leftarrow 1$	2.6	1.3×10^{-3} cm^{-1}	MW	54	200 kHz	3.6	0.64
IR	852	$3 \leftarrow 2$	9.1	4.5×10^{-3} cm^{-1}	MW	441	1 MHz	1.8	1.84
IR	1448	$2 \leftarrow 0$	4.4	2.2×10^{-3} cm^{-1}					
IR	1396	$3 \leftarrow 1$	8.0	4.0×10^{-3} cm^{-1}					
IR	150	$4 \leftarrow 2$	49.3	24.6×10^{-3} cm^{-1}					
IR	2446	$v_{10} \leftarrow 0$	17.9	5.6×10^{-3} cm^{-1}					

[a] The left side of this table gives an overview of transitions separated into microwave (MW) and infrared (IR), and labeled by upper and lower state torsional quantum numbers v_t' and v_t''.

[b] Number of transitions in each category.

[c] Weighted root-mean-square deviation of transitions in each category.

[d] Root-mean-square deviation in measurement units for transitions in each category.

[e] The right side of this table gives an overview of MW transitions, grouped by measurement uncertainty.

[f] Measurement uncertainties assigned to MW transitions in this fit. Weight used in the fit = (Meas. Unc.)$^{-2}$. The category labeled 45 kHz contains lines with uncertainties of 40 and 50 kHz.

The $K = 5$ levels of v_{10} (near 623 cm^{-1} in Fig. 4) appear to exhibit relatively localized avoided crossings at $J \approx 8.5$ and $J \approx 14.5$ with the set of bath-state $K = 8$ levels connected to the dashed parabola. The $K = 7$ levels of v_{10} near 660 cm^{-1} appear to participate in a stronger and less localized avoided crossing with bath-state $K = 5$ levels connected to the dashed parabola. Given the presence of these and other similar $\Delta K \neq 0$ interactions, we tried to reduce residuals in our fit by adding a number of $\Delta K > 0$ interaction terms, but this led to unstable fits with little improvement in standard deviation. It is probable that accurate experimental values, rather than extrapolated calculated values, for the numerous bath-state levels in Fig. 4 will be required in order to proceed further with this analysis.

Figs. 5 and 6 show the reduced energy positions, $E - 0.3J(J + 1)$, of all E-species torsion–rotation levels with $J \leqslant 18$ lying in the energy range from 570 to 720 cm^{-1}, as calculated from our fitting parameters. The energy scale in these figures for E states is twice as large as that for A states in Fig. 4, because of the increased congestion caused by splitting of higher-v_t E levels into $mK > 0$ and $mK < 0$ components. Figs. 5 and 6 include v_{10} E levels with $0 \leqslant |K| \leqslant 9$, which are again shown as black squares connected by thick black lines. Based on the vibrational ground state parameters, intrinsic torsional splittings in v_{10} should be smaller than 0.1 cm^{-1}, so that the v_{10} E levels in Figs. 5 and 6 should, in the absence of significant perturbations from neighboring bath states, behave like ordinary asymmetric rotor levels, with torsional splittings unresolved on the scale of Figs. 5 and 6. Levels of $v_t = 1$ and 2 are plotted as small green circles connected by thin green lines, but the color coding for the other levels differs from that in Fig. 4. In particular, levels of $v_t = 3$ are plotted in orange, and are labeled by the sign of their σ value followed by their K value (see Fig. 3). Levels of $v_t = 4$ are plotted in blue, and are also labeled by σK. These are the levels expected to interact most strongly with the v_{10} levels, since close-lying J-series can have matching σK values. Levels of $v_t = 5$ (only in Fig. 6) are plotted in purple and labeled by σK. (Note that these signed K values (i.e., these σK values) are the same as those discussed in [20] and used in our fitting program, but they are not the same as a notation using the sign of mK followed by K.)

The survey in Fig. 3 indicates that v_{10} E states with $\sigma K = 0$, +3, −6, and ±9 lie close in energy to bath states with the same K values, which, in Figs. 5 and 6 as in Fig. 4, are indicated by the blue symbols ×. As mentioned earlier, we were unable to identify convincingly any lines from v_{10} E-species series with $\sigma K = 0$, +1, and −1. Fig. 5 shows that the two $|K| = 1$ series of v_{10} E levels near 585 cm^{-1} are calculated to be nearly degenerate with a $K = 0$ series

of torsional bath states (- × -). We believe that interactions among these levels have prevented us from locating the $\sigma K = 0$ and ±1 v_{10} E levels in the dense band center region. Similarly, the E levels of v_{10} with $\sigma K = +3$ near 597 cm^{-1} in Fig. 5 are significantly perturbed by the $\sigma K = +3$ bath level (- × -) calculated to lie about 3 cm^{-1} higher, but the resulting displacements (some more than 1 cm^{-1}) are reasonably well accounted for by the present model, since residuals for transitions to the v_{10} $\sigma K = +3$ levels are less than 0.013 cm^{-1}, as shown in Table 7. The v_{10} $|K| = 6$ levels near 640 cm^{-1}, are split by about 0.4 cm^{-1}, presumably because of interaction with the $\sigma K = -6$ bath level (- × -) near 635 cm^{-1}. This splitting is also reasonably well accounted for in the present model, since residuals for transitions to the v_{10} $\sigma K = -6$ levels in Table 7 have magnitudes of 0.010 cm^{-1} or less. For comparison, the presumably much less perturbed $\sigma K = -3$ and +6 counterparts to the levels above exhibit residuals of 0.004 cm^{-1} or less for $J \leqslant 14$. The v_{10} $\sigma K = +9$ and −9 levels with $9 \leqslant J \leqslant 15$ near 715 cm^{-1} in Fig. 6 are split by amounts ranging from 0.2 to 0.6 cm^{-1}, presumably because of $\Delta K = 0$ interactions with both the $\sigma K = +9$ series (- × -) beginning near 703 cm^{-1} and the $\sigma K = -9$ series (- × -) beginning near 711 cm^{-1}, as well as because of crossings with a $\sigma K = -10$ and a $\sigma K = -11$ series. These rather complicated perturbations are reasonably well accounted for in the present model, since residuals for the v_{10} $|K| = 9$ levels are 0.016 cm^{-1} or less.

The v_{10} fitting situation can be approximately summarized as follows. Some v_{10} A and E levels with $|K| = 3$, 6 or 9 are shifted by amounts of the order of 1 cm^{-1}, almost certainly because of the $\Delta K = 0$ interactions with the torsional bath predicted by the energy level overview in Fig. 3. These large $\Delta K = 0$ shifts, together with some smaller ones arising from $\Delta K \neq 0$ interactions, are relatively well accounted for in the present fit, since the magnitudes of most v_{10} obs − calc residuals are 0.01 cm^{-1} or less.

5.3. Molecular constants

We now discuss molecular constants from the present fit from three points of view: (i) Torsion–rotation constants for the ground vibrational state from the present fit can be compared with those from earlier fits. (ii) Torsion–rotation constants for the v_{10} state can be compared with those for the ground vibrational state. (iii) Coefficients of terms describing interactions between v_{10} and the torsional bath states can be related to the observed perturbations. Thus, Table 2 contains three columns of second- and fourth-order torsion–rotation fitting constants for acetaldehyde. The first column is taken from the ground state fit of Ref. [1], which included

Table 6

Assignments[a], observed wavenumbers[b] in cm^{-1}, and observed-minus-calculated residuals[c] $\times 10^3$ in cm^{-1} for the $K = 3$ and $K = 6$[d] A-species subbands of the ν_{10} vibrational band

Table 6 (continued)

J'	K'$_a$	K'$_c$	P'	J''	K''$_a$	K''$_c$	P''	Wavenumber[b]	O-C[c]
3	3	1	+	2	2	0	+	518.68431	−0.8
3	3	1	+	3	2	2	−	516.75682	−1.2
3	3	1	+	3	3	0	−	508.89252	−1.0
3	3	1	+	4	3	2	+	506.32057	−1.7
3	3	1	+	4	4	0	+	495.33605	−1.2
3	3	0	−	2	2	1	−	518.68367	−2.1
3	3	0	−	3	2	1	+	516.75405	−1.0
3	3	0	−	4	2	3	−	514.18680	−1.5
3	3	0	−	3	3	1	+	508.89234	−1.2
3	3	0	−	4	3	1	−	506.32073	−1.5
3	3	0	−	4	4	1	−	495.33558	−1.6
4	3	2	+	3	2	1	+	519.31833	−0.8
4	3	2	+	4	2	3	−	516.75088	−1.5
4	3	2	+	3	3	1	+	511.45541	−2.2
4	3	2	+	4	3	1	−	508.88472	−1.6
4	3	2	+	5	3	3	+	505.67041	−1.5
4	3	2	+	4	4	1	−	497.89958	−1.7
4	3	2	+	5	4	1	+	494.68608	−1.5
4	3	1	−	3	2	2	−	519.32082	−1.3
4	3	1	−	4	2	2	+	516.74182	−1.6
4	3	1	−	3	3	0	−	511.45603	−1.6
4	3	1	−	4	3	2	+	508.88570	−0.7
4	3	1	−	5	3	2	−	505.67024	−1.5
4	3	1	−	4	4	0	+	497.89981	−1.5
4	3	1	−	5	4	2	−	494.68636	−1.3
5	3	3	+	4	2	2	+	519.94774	−1.2
5	3	3	+	5	2	4	−	516.74530	−1.3
5	3	3	+	6	2	4	−	512.85069	−1.7
5	3	3	+	4	3	2	+	512.08996	−2.0
5	3	3	+	5	3	2	−	508.87598	−1.3
5	3	3	+	6	3	4	+	505.01783	−1.6
5	3	3	+	4	4	0	+	501.10587	−1.0
5	3	3	+	5	4	2	−	497.89206	−1.1
5	3	3	+	6	4	2	+	494.03551	−0.9
5	3	2	−	4	2	3	−	519.95717	−1.0
5	3	2	−	5	2	3	+	516.72415	−1.7
5	3	2	−	6	2	5	−	512.89209	−2.2
5	3	2	−	4	3	1	−	512.09090	−1.1
5	3	2	−	5	3	3	+	508.87622	−1.4
5	3	2	−	6	3	3	−	505.01815	−0.9
5	3	2	−	4	4	1	−	501.10589	−1.1
5	3	2	−	5	4	1	+	497.89190	−1.4
5	3	2	−	6	4	3	−	494.03586	−0.7
6	3	4	+	5	2	3	+	520.57232	−0.8
6	3	4	+	6	2	5	−	516.73998	−1.6
6	3	4	+	7	2	5	+	512.17209	−1.7
6	3	4	+	5	3	3	+	512.72404	−0.8
6	3	4	+	6	3	3	−	508.86454	−1.8
6	3	4	+	7	3	5	+	504.36343	−1.5
6	3	4	+	5	4	1	+	501.73903	−1.6
6	3	4	+	6	4	3	−	497.88266	−1.2
6	3	4	+	7	4	3	+	493.38268	−1.1
6	3	3	−	5	2	4	−	520.59404	−0.4
6	3	3	−	6	2	4	+	516.69926	−1.0
6	3	3	−	5	3	2	−	512.72498	−0.1
6	3	3	−	6	3	4	+	508.86706	−0.2
6	3	3	−	7	3	4	−	504.36375	−0.6
6	3	3	−	6	4	2	+	497.88421	−0.1
6	3	3	−	7	4	4	−	493.38437	0.2
7	3	5	+	6	2	4	+	521.18778	−1.6
7	3	5	+	7	2	6	−	516.73675	−1.5
7	3	5	+	8	2	6	+	511.48065	−1.1
7	3	5	+	6	3	4	+	513.35545	−1.0
7	3	5	+	7	3	4	−	508.85342	0.2
7	3	5	+	8	3	6	+	503.70719	−1.3
7	3	5	+	7	4	4	−	497.87239	−1.0
7	3	5	+	8	4	4	+	492.72903	−0.7
7	3	4	−	6	2	5	−	521.22926	−3.0
7	3	4	−	7	2	5	+	516.66155	−2.9
7	3	4	−	8	2	7	−	511.60455	−2.1
7	3	4	−	6	3	3	−	513.35497	−2.0
7	3	4	−	7	3	5	+	508.85354	−2.1
7	3	4	−	8	3	5	−	503.70454	−2.1
7	3	4	−	6	4	3	−	502.37195	−2.6
7	3	4	−	7	4	3	+	497.87153	−2.9
7	3	4	−	8	4	5	−	492.72867	−2.2
8	3	6	+	7	2	5	+	521.79435	−1.1
8	3	6	+	8	2	7	−	516.73675	−0.9
8	3	6	+	9	2	7	+	510.77199	−1.5
8	3	6	+	7	3	5	+	513.98489	−1.7
8	3	6	+	8	3	5	−	508.83594	−1.7
8	3	6	+	9	3	7	+	503.04894	−1.1
8	3	6	+	7	4	3	+	503.00379	−1.7
8	3	6	+	8	4	5	−	497.86048	−1.4
8	3	6	+	9	4	5	+	492.07320	−1.2
8	3	5	−	7	2	6	−	521.87098	−1.7
8	3	5	−	8	2	6	+	516.61491	−1.3
8	3	5	−	9	2	8	−	510.96671	−1.9
8	3	5	−	7	3	4	−	513.98612	−1.6
8	3	5	−	8	3	6	+	508.84203	−0.9
8	3	5	−	9	3	6	−	503.04528	−1.3
8	3	5	−	7	4	4	−	503.00655	−1.3
8	3	5	−	8	4	4	+	497.86285	−1.4
8	3	5	−	9	4	6	−	492.07569	−1.2
9	3	7	+	8	2	6	+	522.38851	−0.3
9	3	7	+	9	2	8	−	516.74097	−0.2
9	3	7	+	10	2	8	+	510.04580	−0.5
9	3	7	+	8	3	6	+	514.61544	−0.1
9	3	7	+	10	3	8	+	502.38869	−1.2
9	3	7	+	9	4	6	+	497.84870	−0.8
9	3	7	+	10	4	6	+	491.41701	−0.9
9	3	6	−	8	2	7	−	522.51586	−1.6
9	3	6	−	9	2	7	+	516.55185	−1.4
9	3	6	−	10	2	9	−	510.33537	−1.1
9	3	6	−	8	3	5	−	514.61582	−1.6
9	3	6	−	9	3	7	+	508.82848	−1.4
9	3	6	−	10	3	7	−	502.38171	−2.1
9	3	6	−	9	4	5	+	497.85250	−1.7
9	3	6	−	10	4	7	−	491.42134	−1.5
10	3	8	+	9	2	7	+	522.96546	−1.2
10	3	8	+	10	2	9	−	516.74844	−1.5
10	3	8	+	11	2	9	+	509.29741	−0.7
10	3	8	+	9	3	7	+	515.24215	−1.2
10	3	8	+	11	3	9	+	501.72629	−1.7
10	3	8	+	9	4	5	+	504.26668	−1.0
10	3	8	+	10	4	7	−	497.83555	−0.7
10	3	8	+	11	4	7	+	490.75883	−1.2
10	3	7	−	9	2	8	−	523.16677	−1.4
10	3	7	−	10	2	8	+	516.47256	−0.8
10	3	7	−	11	2	10	−	509.71136	−1.1
10	3	7	−	9	3	6	−	515.24510	−1.2
10	3	7	−	10	3	8	+	508.81497	−1.9
10	3	7	−	11	3	8	−	501.71659	−1.3
10	3	7	−	9	4	6	−	504.27587	−0.7
10	3	7	−	10	4	6	+	497.84368	−1.2
10	3	7	−	11	4	8	−	490.76812	−1.1
11	3	9	+	10	2	8	+	523.52548	−0.9
11	3	9	+	11	2	10	−	516.76429	−1.2
11	3	9	+	12	2	10	+	508.52613	−0.9
11	3	9	+	10	3	8	+	515.86836	−1.5
11	3	9	+	11	3	8	−	508.77003	−0.9
11	3	9	+	12	3	10	+	501.06332	−1.3
11	3	9	+	10	4	6	+	504.89725	−0.7
11	3	9	+	11	4	8	−	497.82113	−1.1
11	3	9	+	12	4	8	+	490.09965	−1.3
11	3	8	−	10	2	9	−	523.82650	−0.6
11	3	8	−	11	2	9	+	516.37396	−1.3
11	3	8	−	12	2	11	−	509.09792	−0.8
11	3	8	−	10	3	7	−	515.87315	−1.2
11	3	8	−	11	3	9	+	508.80381	−1.3
11	3	8	−	12	3	9	−	501.04732	−1.2
11	3	8	−	10	4	7	−	504.91198	−1.4
11	3	8	−	11	4	7	+	497.83623	−1.0
11	3	8	−	12	4	9	−	490.11575	−1.2
12	3	10	+	11	2	9	+	524.06414	−1.5
12	3	10	+	12	2	11	−	516.78761	−1.5
12	3	10	+	13	2	11	+	507.72992	−1.8
12	3	10	+	11	3	9	+	516.49427	−1.2
12	3	10	+	12	3	9	−	508.73763	−1.3

Table 6 (continued)

J'	K'a	K'c	P'	J''	K''a	K''c	P''	Wavenumber[b]	O-C[c]
12	3	10	+	13	3	11	+	500.39859	−1.4
12	3	10	+	11	4	7	+	505.52574	−1.8
12	3	10	+	12	4	9	−	497.80575	−1.6
12	3	10	+	13	4	9	+	489.43900	−1.4
12	3	9	−	11	2	10	−	524.49533	−1.1
12	3	9	−	12	2	10	+	516.25610	−1.9
12	3	9	−	11	3	8	−	516.49998	−1.9
12	3	9	−	12	3	10	+	508.79354	−2.0
12	3	9	−	13	3	10	−	500.37431	−1.1
12	3	9	−	11	4	8	−	505.55195	−1.3
12	3	9	−	12	4	8	+	497.83104	−0.9
12	3	9	−	13	4	10	−	489.46589	−1.1
13	3	11	+	12	2	10	+	524.58097	−1.4
13	3	11	+	13	2	12	−	516.82095	−1.4
13	3	11	+	14	2	12	+	506.91016	−1.8
13	3	11	+	12	3	10	+	517.11843	−1.6
13	3	11	+	13	3	10	−	508.69861	−1.3
13	3	11	+	14	3	12	+	499.73274	−1.7
13	3	11	+	12	4	8	+	506.15455	−1.8
13	3	11	+	13	4	10	−	497.78977	−1.7
13	3	11	+	14	4	10	+	488.77640	−1.5
13	3	10	−	12	2	11	−	525.17826	−0.7
13	3	10	−	13	2	11	+	516.12016	−1.5
13	3	10	−	14	2	13	−	507.91110	−1.6
13	3	10	−	12	3	9	−	517.12773	−1.1
13	3	10	−	13	3	11	+	508.78853	−1.3
13	3	10	−	14	3	11	−	499.69673	−1.4
13	3	10	−	12	4	9	−	506.19587	−1.4
13	3	10	−	13	4	9	+	497.82902	−1.2
13	3	10	−	14	4	11	−	488.81904	−1.5
14	3	12	+	13	2	11	+	525.07400	−1.5
14	3	12	+	14	2	13	−	516.86490	−1.7
14	3	12	+	15	2	13	+	506.06605	−1.8
14	3	12	+	13	3	11	+	517.74210	−1.6
14	3	12	+	14	3	11	−	508.64967	−2.3
14	3	12	+	15	3	13	+	499.06584	−2.5
14	3	12	+	13	4	9	+	506.78274	−1.4
14	3	12	+	14	4	11	−	497.77200	−2.4
14	3	12	+	15	4	11	+	488.11091	−2.4
14	3	11	−	13	2	12	−	525.87642	−1.2
14	3	11	−	14	2	12	+	515.96603	−1.3
14	3	11	−	15	2	14	−	507.34423	−2.2
14	3	11	−	13	3	10	−	517.75368	−1.6
14	3	11	−	14	3	12	+	508.78853	−1.3
14	3	11	−	15	3	12	−	499.01460	−1.5
14	3	11	−	13	4	10	−	506.84498	−1.8
14	3	11	−	14	4	10	+	497.83125	−2.1
15	3	13	+	14	2	12	+	525.54279	−1.5
15	3	13	+	15	2	14	−	516.92155	−1.8
15	3	13	+	14	3	12	+	518.36493	−1.9
15	3	13	+	15	3	12	-	508.59121	−1.8
15	3	13	+	14	4	10	+	507.40818	−2.1
15	3	13	+	15	4	12	−	497.75354	−2.3
15	3	12	−	14	2	13	-	526.59504	−0.7
15	3	12	−	15	2	13	+	515.79535	−1.7
15	3	12	−	14	3	11	−	518.37949	-1.7
15	3	12	−	15	3	13	+	508.79686	−0.7
15	3	12	−	15	4	11	+	497.84090	−1.6
6	6	0	+	5	5	1	+	528.10941	−9.7
6	6	0	+	6	6	1	−	507.04984	−10.1
6	6	0	+	7	6	1	+	502.55166	−9.4
6	6	0	+	7	7	1	+	482.23623	−9.2
7	6	1	+	6	5	2	+	529.09345	−14.9
7	6	1	+	7	5	2	−	524.59378	−15.4
7	6	1	+	8	5	4	+	519.45159	−15.4
7	6	1	+	6	6	0	+	511.89053	−14.9
7	6	1	+	7	6	2	−	507.39141	−15.1
7	6	1	+	8	6	2	+	502.24944	−15.3
7	6	1	+	7	7	0	−	487.07561	−15.3
7	6	1	+	8	7	2	+	481.93389	−15.3
8	6	2	+	7	5	3	+	530.06847	−12.8
8	6	2	+	8	5	3	−	524.92655	−12.5
8	6	2	+	9	5	5	+	519.14118	−12.3
8	6	2	+	7	6	1	+	512.86541	−13.1
8	6	2	+	8	6	3	−	507.72359	−13.2
8	6	2	+	9	6	3	+	501.93864	−13.3

Table 6 (continued)

J'	K'a	K'c	P'	J''	K''a	K''c	P''	Wavenumber[b]	O-C[c]
8	6	2	+	7	7	1	+	492.54986	−13.1
8	6	2	+	8	7	1	−	487.40850	−12.7
8	6	2	+	9	7	3	+	481.62388	−12.8
9	6	3	+	8	5	4	+	531.08555	−1.7
9	6	3	+	9	5	4	−	525.29951	−2.2
9	6	3	+	10	5	6	+	518.87069	−2.1
9	6	3	+	8	6	2	+	513.88302	−2.0
9	6	3	+	9	6	4	−	508.09795	−2.3
9	6	3	+	10	6	4	+	501.67102	−1.4
9	6	3	+	8	7	2	+	493.56754	−1.9
9	6	3	+	9	7	2	−	487.78299	−1.9
9	6	3	+	10	7	4	+	481.35519	−2.2
10	6	4	+	9	5	5	+	531.98091	−6.2
10	6	4	+	10	5	5	−	525.55211	−6.1
10	6	4	+	11	5	7	+	518.47987	−5.8
10	6	4	+	9	6	3	+	514.77904	−6.6
10	6	4	+	10	6	5	−	508.35129	−6.5
10	6	4	+	11	6	5	+	501.28010	−6.6
10	6	4	+	9	7	3	+	494.46385	−6.4
10	6	4	+	10	7	3	−	488.03576	−7.0
10	6	4	+	11	7	5	+	480.96559	−6.7

[a] Asymmetric rotor quantum numbers J, K_a, K_c for the upper (′) and lower (″) states augmented by a parity quantum number P defined in Ref. [1].

[b] Measurement error (type B, $k = 1$) [23] is estimated to be 0.00032 cm^{-1}.

[c] From our fit of 10 587 lines (see Tables 2–5 and the text).

[d] Even though the K_a' = 3 upper state levels in this table are perturbed by about 1 cm^{-1} (see text and Fig. 4), they can be fit by the present model to about 0.002 cm^{-1}. The K_a' = 6 levels are also strongly perturbed, but this perturbation is less well accounted for, since residuals for J' = 6, 7, and 8 reach 0.015 cm^{-1} in magnitude.

a (non-uniform) distribution of rotational levels up to $K = 14$, $J = 26$ and torsional levels up to $v_t = 4$. The second column gives ground state constants from the present fit, which includes a non-uniform distribution of rotational levels up to $K = 13$, $J = 15$ and torsional levels up to $v_t = 4$. The third column gives constants for the v_{10} vibrational state from the present fit, which includes a relatively uniform distribution of rotational levels up to $K = 9$, $J = 15$ and torsional levels of v_{10} with $v_t = 0$ only. Similarly, Table 3 contains two columns of sixth-order fitting constants; the third column is missing here, since no sixth-order constants were used for the v_{10} vibrational state. Table 4 presents the v_{10}-torsional-bath interaction constants.

Ground state constants from the present fit in Tables 2 and 3 can be divided into two groups: one group was floated; the other group, which contains most of the constants required by high-J levels, was kept fixed, either at values from the fit in Ref. [1], or at values from some earlier fit. (It is, of course, not clear at the moment whether keeping any particular higher-order v_{10} constant fixed at its ground state value is a better approximation than setting it to zero, but on the average the former approximation seems preferable.) In any case, it can be seen from Table 2 that the lowest-order (i.e., $n = 2$) ground state constants did not change dramatically from their earlier values. The same remark is true for most constants with $n = 4$, with the notable exception of the parameter k_7, which changes sign and decreases in magnitude by a factor of 3.6. Most of the $n = 6$ constants in Table 3 were fixed at their values from the earlier fit [1], but those that were floated here and then fixed do not change dramatically, except for V_9 and V_{12}, which change sign. Significant changes in these two torsional potential function parameters are probably associated with introduction of the v_{10}-bath interaction parameters.

The torsion–rotation constants for v_{10} given in the third column of Table 2 present a problem because correlation in the least-squares fit between these constants and those for interaction of v_{10} with the torsional bath (given in Table 4) can only be broken if a large number of perturbation-partner bath-state level positions
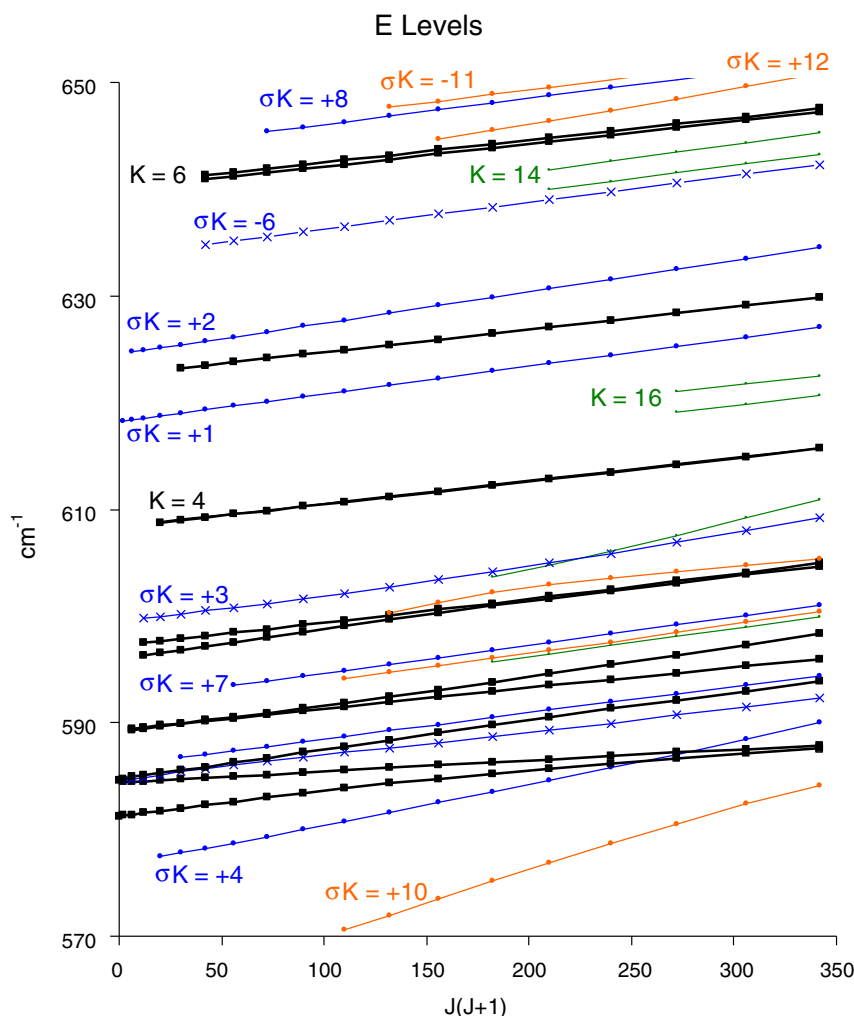
Fig. 5. E-species torsion–rotation energy levels of acetaldehyde in the wavenumber range of 570–650 cm^{-1}, calculated from our global fitting parameters and plotted in the reduced form $E - 0.3J(J+1)$ against $J(J+1)$. (i) Energy levels of the ν_{10} fundamental state ($0 \leqslant |K| \leqslant 6$) are plotted as large black squares connected by heavy black lines. By analogy with the ground torsion–vibration state, these levels are expected, in the absence of perturbations from bath states, to look like asymmetric rotor levels on the scale of Fig. 5. Only the $K = 4$ and 6 series are labeled in this figure. (ii) Energy levels for $\nu_t = 1$, $K = 16$ and $\nu_t = 2$, $K = 13$ and 14 are plotted as small green circles connected by thin green lines. The two $K = 13$ series (between 590 and 610 cm^{-1}) are not labeled. These high-K levels are not expected to interact significantly with the neighboring low-K ν_{10} levels. (iii) Energy levels for $\nu_t = 3$, $\sigma K = +10, -10, +11, +12, -11$ (in order of increasing energy) are plotted as orange circles connected by orange lines. (See also Fig. 3 for torsion-K-rotation levels labeled by ν_t, σ, and K.) These moderate-K levels are also not expected to interact significantly with the neighboring low-K ν_{10} levels. (iv) Energy levels for $\nu_t = 4$, $\sigma K = +4, 0, -5, +7, +3, +1, +2, -6, +8$ (in order of increasing energy) are mostly plotted as blue circles connected by blue lines, but three J-series for $\nu_t = 4$, i.e., those with $\sigma K = 0, +3$ and -6, are plotted as blue $\times$'s connected by blue lines. These levels interact rather strongly with the $\sigma K = 0, +3$ and -6 levels of ν_{10} via terms in the Hamiltonian satisfying $\Delta K = 0$ selection rules. (v) In spite of the high density of levels in this figure, it can be seen that the rotational levels in almost all J-series are connected together by nearly straight lines, indicating that the J-dependence of the rotational energy within each series is well characterized by a nearly constant effective B value. (For interpretation of the references to color in this figure legend, the reader is referred to the web version of this paper.)

are experimentally known, which is not the case. Since the introduction of ν_{10}-bath interaction constants is essential, only a small number of pure ν_{10} constants were used in the fit, and four of these were eventually fixed. The large change in F, V_3, and ρ between the ground state and ν_{10} probably has little physical or structural meaning, since only the lowest state of the torsional manifold built on ν_{10} has been included in the fit.

The most interesting parameters in the present work are those in Table 4, which describe the interaction of ν_{10} (which plays the role of a bright fundamental state) with the torsional bath (which plays the role of an incipient underlying quasi-continuum). These parameters are denoted, when convenient, by symbols for the analogous single-state parameter prefixed by "W." All but one of the interaction parameters used here and given in Table 4 multiply vibration–torsion–rotation operators that obey $\Delta K = 0$ selection rules. Such operators represent purely torsion–vibration interactions together with their $J(J+1)$ and K^2 rotational dependences,

and usually give rise to rather global perturbations which shift all J levels of given K up or down by approximately the same amount. Only the parameter WFB6 multiplies an operator obeying $\Delta K \neq 0$ selection rules. Such operators represent off-diagonal moment-of-inertia and Coriolis effects together with their $J(J+1)$ and K^2 rotational dependences, and usually give rise to rather local perturbations affecting a few J levels of given K in an avoided-crossing situation. They also introduce considerable instability in the least-squares procedure, particular when the energies of one of the perturbation partner series are not known experimentally, so we floated only one parameter of this type in the present fit.

Consider first the purely torsion–vibration (i.e., anharmonic) interaction terms. These are all of the form $Q_{10}\cos 3n\gamma$ in the present fit, with selection rules $\Delta\nu_{10} = \pm 1$ and $\Delta K = 0$, and with coefficients called WC3, WC6, and WC9. As discussed earlier, Fig. 3 suggests that the largest interactions satisfying these selection rules (and for states with $|K| \leqslant 9$) will take place for A states with
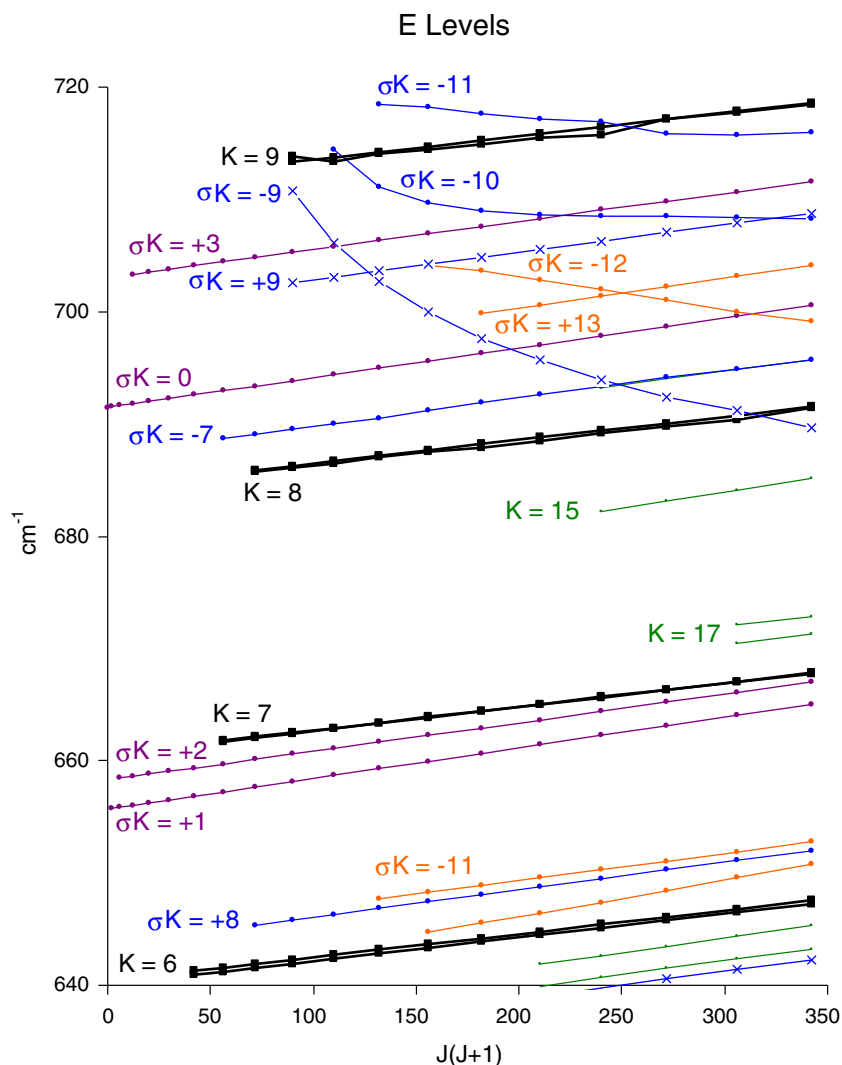
Fig. 6. A continuation of the E-species torsion–rotation energy levels of acetaldehyde from Fig. 5 into the wavenumber range from 640 to 720 cm^{-1}, calculated from our global fitting parameters and plotted in the reduced form $E-0.3J(J+1)$ against $J(J+1)$. The symbols and color coding are almost the same as in Fig. 5. (i) Energy levels of the ν_{10} fundamental state ($6 \leqslant |K| \leqslant 9$) are plotted as black squares connected by heavy black lines. These levels are expected, in the absence of perturbations from bath states, to look like asymmetric rotor levels on the scale of Fig. 6. (ii) Energy levels for $\nu_t = 1$, $K = 17$ and $\nu_t = 2$, $K = 14$ and 15 are plotted as small green circles connected by thin green lines. The two $K = 14$ series are not labeled. (iii) Energy levels for $\nu_t = 3$, $\sigma K = +12$, -11, $+13$, -12 (in order of increasing energy) are plotted as orange circles connected by orange lines. (iv) Energy levels for $\nu_t = 4$, $\sigma K = +8$, -7, $+9$, -9, -10, -11 (in order of increasing energy) are mostly plotted as blue circles connected by blue lines, but two J-series for $\nu_t = 4$, i.e., those with $\sigma K = +9$ and -9 are plotted as blue × 's connected by blue lines. These levels interact rather strongly with the $K = 9$ levels of ν_{10} via terms in the Hamiltonian satisfying $\Delta K = 0$ selection rules. (v) Energy levels for $\nu_t = 5$, $\sigma K = +1$, $+2$, 0, $+3$ (in order of increasing energy) are plotted as purple circles connected by purple lines, (vi) Rotational levels in the $\nu_t = 4$ J-series with $\sigma K = -9$, -10, and -11 exhibit rapidly varying effective B values. Note in addition the two level crossings affecting the ν_{10} $|K| = 9$ levels in the 715 cm^{-1} region. (For interpretation of the references to color in this figure legend, the reader is referred to the web version of this paper.)

$K = 3$ and 6 and for E states with $\sigma K = 0$, $+3$, -6, and ±9. We observed only six of these seven interactions, since $K = 0$ E-species transitions were not identified, and found magnitudes for the global level shifts of the order of 0.5–1 cm^{-1}. In the present fit we have used the three lowest-order terms to describe these six interactions, i.e., $Q_{10}\cos3\gamma$, $Q_{10}\cos6\gamma$, and $Q_{10}\cos9\gamma$. The global shifts are described rather well, i.e., to better than 0.01 cm^{-1}, but the coefficients required are approximately $+5$, -11, and $+14$ cm^{-1}, showing that the Fourier series representation of this part of the potential surface is not rapidly convergent.

Consider finally the term WFB6, with selection rules $\Delta \nu_{10} = \pm1$ and $\Delta K = \pm1$. We examined a large number of trial-and-error sets of $\Delta K \neq 0$ terms, all of which led to very poorly convergent (or divergent) fits with highly correlated parameters. Thus this term is essentially an effective parameter performing avoided crossing perturbations for a variety of other terms not determinable from the present data set.

6. Future work

Even though the Hamiltonian and fitting parameters determined in this work have led to a significant increase in our understanding of the interactions between the ν_{10} bright state and the dark torsional bath in which it is embedded, it is clear that future work must aim at removing many of the ambiguities remaining in the present global fit. In the authors' opinion, further progress cannot be achieved with the present data set (in spite of the fact that it contains over 10 500 transitions), because transitions to many of the perturbation-partner states have not been identified. The lack of such perturbation-partner information makes it essentially impossible to carry out a proper least-squares fit.

One promising approach to increasing the data set is suggested by the recent study of acetamide [24], where approximately 1600 torsion–rotation lines with J up to 20, K_a up to 11, and $\nu_t \leqslant 2$ were measured on a room-temperature sample be-

Table 7

Assignments[a], observed wavenumbers[b] in cm^{-1}, and observed-minus-calculated residuals[c] × 10^3 in cm^{-1} for the K = +3 and −6[d] E-species subbands of the ν_{10} vibrational band

J'	K'$_a$	K'$_c$	J''	K''$_a$	K''$_c$	Wavenumber[b]	O–C[c]
3	3	0	2	2	0	516.38915	1.7
3	3	0	3	2	1	514.46136	2.5
3	3	0	3	3	0	506.64638	1.0
3	3	0	4	3	1	504.07653	2.4
3	3	0	4	4	0	493.14158	1.5
4	3	1	3	2	1	517.10269	0.6
4	3	1	4	2	2	514.52988	0.4
4	3	1	5	2	3	511.31164	0.2
4	3	1	3	3	0	509.28882	0.1
4	3	1	4	3	1	506.71405	−3.4
4	3	1	5	3	2	503.50292	−0.1
4	3	1	4	4	0	495.78402	0.6
4	3	1	5	4	1	492.56933	−0.1
5	3	2	4	2	2	517.83029	−1.4
5	3	2	5	2	3	514.61136	−2.3
5	3	2	6	2	4	510.74563	−1.6
5	3	2	4	3	1	510.01718	−2.5
5	3	2	5	3	2	506.80288	−2.3
5	3	2	6	3	3	502.94554	−1.5
5	3	2	4	4	0	499.08440	−1.2
5	3	2	5	4	1	495.87009	−1.5
5	3	2	6	4	2	492.01279	−1.6
6	3	3	5	2	3	518.56959	−3.6
6	3	3	6	2	4	514.70243	−4.4
6	3	3	5	3	2	510.76068	−4.1
6	3	3	6	3	3	506.90288	−3.7
6	3	3	7	3	4	502.40066	−3.7
6	3	3	6	4	2	495.96990	−4.1
6	3	3	7	4	3	491.46948	−4.0
7	3	4	6	2	4	519.31605	−5.8
7	3	4	7	2	5	514.79690	−5.9
7	3	4	8	2	6	509.62111	−5.5
7	3	4	6	3	3	511.51651	−5.1
7	3	4	7	3	4	507.01359	−5.8
7	3	4	8	3	5	501.86671	−5.9
7	3	4	6	4	2	500.58276	−6.2
7	3	4	7	4	3	496.08291	−5.6
7	3	4	8	4	4	490.93853	−5.8
8	3	5	7	2	5	520.06240	−8.4
8	3	5	8	2	6	514.88653	−8.0
8	3	5	9	2	7	509.04936	−8.4
8	3	5	7	3	4	512.27893	−8.4
8	3	5	8	3	5	507.13232	−8.2
8	3	5	9	3	6	501.34098	−7.6
8	3	5	8	4	4	496.20384	−8.5
8	3	5	9	4	5	490.41614	−8.2
9	3	6	8	2	6	520.80268	−9.7
9	3	6	9	2	7	514.96560	−10.0
9	3	6	10	2	8	508.46595	−9.8
9	3	6	8	3	5	513.04881	−9.6
9	3	6	9	3	6	507.25623	−10.3
9	3	6	10	3	7	500.81856	−10.0
9	3	6	8	4	4	502.12009	−10.1
9	3	6	9	4	5	496.33197	−10.2
9	3	6	10	4	6	489.89992	−10.2
10	3	7	9	2	7	521.52795	−11.8
10	3	7	10	2	8	515.02835	−11.6
10	3	7	9	3	6	513.81899	−11.6
10	3	7	10	3	7	507.38112	−11.6
10	3	7	11	3	8	500.29606	−11.8
10	3	7	9	4	5	502.89394	−12.4
10	3	7	10	4	6	496.46261	−11.6
10	3	7	11	4	7	489.38598	−11.6
6	−6	0	7	−7	0	484.04575	−0.5
6	−6	0	6	−6	0	508.91195	−0.3
6	−6	0	7	−6	1	504.41306	−0.1
6	−6	0	5	−5	0	530.02035	0.0
6	−6	0	6	−5	1	526.16332	−0.3
6	−6	0	7	−5	2	521.66396	0.1
7	−6	1	8	−7	1	483.39471	−0.8
7	−6	1	6	−6	0	513.40159	−1.2
7	−6	1	7	−6	1	508.90290	−0.8
7	−6	1	8	−6	2	503.76099	−0.8
7	−6	1	6	−5	1	530.65354	−0.7
7	−6	1	7	−5	2	526.15350	−0.9

Table 7 (continued)

J'	K'$_a$	K'$_c$	J''	K''$_a$	K''$_c$	Wavenumber[b]	O–C[c]
7	−6	1	8	−5	3	521.01093	−0.5
8	−6	2	8	−7	1	488.52647	−1.4
8	−6	2	9	−7	2	482.74207	−1.7
8	−6	2	7	−6	1	514.03503	−1.0
8	−6	2	8	−6	2	508.89252	−1.6
8	−6	2	9	−6	3	503.10771	−1.4
8	−6	2	7	−5	2	531.28538	−1.3
8	−6	2	8	−5	3	526.14215	−1.6
8	−6	2	9	−5	4	520.35599	−1.4
9	−6	3	8	−7	1	494.29923	−2.9
9	−6	3	9	−7	2	488.51520	−2.8
9	−6	3	10	−7	3	482.08839	−2.7
9	−6	3	8	−6	2	514.66562	−2.7
9	−6	3	9	−6	3	508.88058	−2.8
9	−6	3	10	−6	4	502.45281	−2.5
9	−6	3	8	−5	3	531.91570	−2.3
9	−6	3	9	−5	4	526.12843	−3.2
9	−6	3	10	−5	5	519.69965	−2.1
10	−6	4	9	−7	2	494.93116	−3.1
10	−6	4	10	−7	3	488.50474	−2.6
10	−6	4	11	−7	4	481.43423	−3.2
10	−6	4	9	−6	3	515.29636	−3.2
10	−6	4	10	−6	4	508.86858	−2.9
10	−6	4	11	−6	5	501.79709	−3.1
10	−6	4	9	−5	4	532.54523	−2.7
10	−6	4	10	−5	5	526.11469	−3.4
10	−6	4	11	−5	6	519.04184	−2.7
11	−6	5	10	−7	3	495.56149	−4.3
11	−6	5	11	−7	4	488.49174	−4.2
11	−6	5	12	−7	5	480.77811	−4.9
11	−6	5	10	−6	4	515.92560	−4.4
11	−6	5	11	−6	5	508.85454	−4.1
11	−6	5	12	−6	6	501.13953	−4.5
11	−6	5	10	−5	5	533.17222	−4.3
11	−6	5	11	−5	6	526.09831	−4.6
11	−6	5	12	−5	7	518.38159	−3.9
12	−6	6	11	−7	4	496.19024	−6.4
12	−6	6	12	−7	5	488.47842	−5.4
12	−6	6	13	−7	6	480.12184	−6.1
12	−6	6	11	−6	5	516.55342	−6.0
12	−6	6	12	−6	6	508.83904	−5.7
12	−6	6	13	−6	7	500.48107	−5.6
12	−6	6	11	−5	6	533.79817	−5.5
12	−6	6	12	−5	7	526.08104	−5.2
12	−6	6	13	−5	8	517.71923	−5.5
13	−6	7	12	−7	5	496.82067	−6.4
13	−6	7	13	−7	6	488.46479	−6.4
13	−6	7	14	−7	7	479.46573	−6.4
13	−6	7	12	−6	6	517.18171	−6.3
13	−6	7	13	−6	7	508.82342	−6.5
13	−6	7	14	−6	8	499.82157	−6.7
13	−6	7	12	−5	7	534.42311	−6.4
13	−6	7	13	−5	8	526.06143	−6.5
13	−6	7	14	−5	9	517.05608	−5.9
14	−6	8	14	−7	7	488.45002	−8.0
14	−6	8	15	−7	8	478.80772	−8.1
14	−6	8	13	−6	7	517.80783	−8.1
14	−6	8	14	−6	8	508.80594	−8.3
14	−6	8	15	−6	9	499.16072	−8.0
14	−6	8	13	−5	8	535.04600	−7.9
14	−6	8	14	−5	9	526.03945	−8.5
14	−6	8	15	−5	10	516.38913	−8.3
15	−6	9	14	−7	7	498.07677	−10.1
15	−6	9	15	−7	8	488.43506	−9.6
15	−6	9	14	−6	8	518.43356	−9.5
15	−6	9	15	−6	9	508.78760	−10.0
15	−6	9	14	−5	9	535.66675	−10.0
15	−6	9	15	−5	10	526.01667	−9.5

[a] Asymmetric rotor quantum numbers J, K_a, K_c for the upper (') and lower ('') states, except that K_a has been given a sign, as defined in Ref. [1].

[b] Measurement error (type B, k = 1) [23] is estimated to be 0.00032 cm^{-1}.

[c] From our fit of 10587 lines (see Tables 2–5 and the text).

[d] Even though the K_a' = +3 upper state levels in this table are perturbed by about 1 cm^{-1} (see text and Fig. 5), they can be fit by the present model to 0.012 cm^{-1} or better. The K_a' = −6 levels are also strongly perturbed, but are again well accounted for, since the residuals are 0.010 cm^{-1} or less. For comparison (see the supplementary material) the presumably less perturbed K_a' = −3 and +6 levels have residuals of 0.004 cm^{-1} or less.

tween 49 and 149 GHz and fit to an accuracy of 25 to 35 kHz. A similar measurement campaign applied to acetaldehyde would greatly improve the accuracy of the microwave measurements presently included in the fit, since only 4% of our present microwave data set of 1746 lines are measured to an accuracy of 20 kHz or better, and 25% are measured to only 1 MHz. In addition, a fully resolved, broad-band, precisely measured room-temperature microwave spectrum would be expected to contain rotational transitions within the ν_{10} fundamental state, as well as rotational transitions within the neighboring torsional bath states, many of which could be unambiguously identified using combination-difference loops.

The acetamide work [24] also led to a relatively simple labeling scheme for torsion–rotation energy levels in the presence of strong ΔK and Δv_t interactions [25]. Although not discussed here, significant labeling difficulties exist also for acetaldehyde [1], particularly in energy regions with irregular J dependences like that near 620 cm^{-1} in Fig. 4. These labeling difficulties make it impossible for the computer program to locate energy levels with a given set of quantum numbers, and they are, in fact, one of the factors preventing us from extending the present fit to J values greater than 15. We are hopeful that the theoretical ideas and algorithms proposed in [25], which deal only with labeling problems in the presence of strong torsion–rotation interaction, can be extended to treat also labeling problems in the presence of the strong vibration–torsion–rotation interactions studied here.

Another promising approach for improving the data set would be to redo the jet-cooled diode laser scans of the ν_{10} fundamental band under conditions which permit full coverage without any frequency gaps, since such a spectrum would almost surely permit secure identification by combination differences of the presently missing E-species subbands involving ν_{10} states with $\sigma K = 0$, +1, and −1. These low-K levels are, of course, essential to stabilizing any large global least-squares fit involving higher-K ν_{10} levels.

Acknowledgments

Appendix A. Supplementary data

Supplementary data for this article consist of the full least-squares fit output, containing over 10 500 infrared and microwave lines, their assignments, and observed-minus-calculated residuals. This output is available on ScienceDirect (www.sciencedirect.com) and as part of the Ohio State University Molecular Spectroscopy Archives (http://library.osu.edu/sites/msa/jmsa_hp.htm). Supplementary data associated with this article can be found, in the online version, at doi:10.1016/j.jms.2008.09.004.

References

[1] I. Kleiner, J.T. Hougen, J.-U. Grabow, S.P. Belov, M.Yu. Tretyakov, J. Cosléou, J. Mol. Spectrosc. 179 (1996) 41–60.
[2] N. Moazzen-Ahmadi, I. Ozier, I. Mukhopadhyay, A.R.W. McKellar, J. Chem. Phys. 108 (1998) 838–848.
[3] S.-X. Wang, J. Schroderus, I. Ozier, N. Moazzen-Ahmadi, V.-M. Horneman, V.V. Ilyushyn, E.A. Alekseev, A.A. Katrich, S.F. Dyubko, J. Mol. Spectrosc. 214 (2002) 69–79.
[4] J. Schroderus, N. Moazzen-Ahmadi, I. Ozier, J. Chem. Phys. 115 (2001) 1392–1404.
[5] J. Schroderus, V.-M. Horneman, M.S. Johnson, N. Moazzen-Ahmadi, I. Ozier, J. Mol. Spectrosc. 215 (2002) 134–143.
[6] N. Moazzen-Ahmadi, J. Mol. Spectrosc. 214 (2002) 144–151.
[7] Certain commercial products are identified in this paper in order to specify adequately the experimental or theoretical procedures. In no case does such identification imply recommendation or endorsement by the National Institute of Standards and Technology, nor does it imply that the products are necessarily the best available for the purpose.
[8] S.W. Sharpe, R. Sheeks, C. Wittig, R.A. Beaudet, Chem. Phys. Lett. 151 (1988) 267–272.
[9] S.W. Sharpe, Y.P. Zeng, C. Wittig, R.A. Beaudet, J. Chem. Phys. 92 (1990) 943–958.
[10] T.A. Hu, E.L. Chappell, S.W. Sharpe, J. Chem. Phys. 98 (1993) 6162–6169.
[11] T.A. Hu, E.L. Chappell, J.T. Munley, S.W. Sharpe, Rev. Sci. Instrum. 64 (1993) 3380–3383.
[12] T.A. Blake, S.W. Sharpe, S.S. Xantheas , J. Chem. Phys. 113 (2000) 707–718.
[13] A.G. Maki, J.S. Wells, Wavenumber Calibration Tables from Heterodyne Frequency Measurements, NIST Special Publication 821, U. S. Government Printing Office, 1991.
[14] G. Moruzzi, L.-H. Xu, R.M. Lees, B.P. Winnewisser, M. Winnewisser, J. Mol. Spectrosc. 167 (1994) 156–175.
[15] J.C.S. Moraes, D. Pereira, A. Scalabrin, G. Moruzzi, F. Strumia, B.P. Winnewisser, M. Winnewisser, I. Mukhopadhyay, P.K. Gupta, J. Mol. Spectrosc. 174 (1995) 177–195.
[16] I. Mukhopadhyay, P.K. Gupta, G. Moruzzi, B.P. Winnewisser, M. Winnewisser, J. Mol. Spectrosc. 186 (1997) 15–21.
[17] G. Moruzzi, W. Jabs, B.P. Winnewisser, M. Winnewisser, J. Mol. Spectrosc. 190 (1998) 353–364.
[18] G. Moruzzi, M. Kunzmann, B.P. Winnewisser, M. Winnewisser, J. Mol. Spectrosc. 219 (2003) 152–162.
[19] G. Moruzzi, Li-Hong Xu, J. Mol. Spectrosc. 165 (1994) 233–248.
[20] J.T. Hougen, I. Kleiner, M. Godefroid, J. Mol. Spectrosc. 163 (1994) 559–586.
[21] E.P. Wigner, Group Theory, Academic Press, New York, 1959.
[22] M.A. Mekhtiev, J.T. Hougen, J. Mol. Spectrosc. 187 (1998) 49–60.
[23] Guidelines for Evaluating and Expressing the Uncertainty of NIST Measurement Results, NIST Technical Note 1297, 1994. Available from http://physics.nist.gov/cuu/Uncertainty/index.html.
[24] V.V. Ilyushin, E.A. Alekseev, S.F. Dyubko, I. Kleiner, J.T. Hougen, J. Mol. Spectrosc. 227 (2004) 115–139.
[25] V. Ilyushin, J. Mol. Spectrosc. 227 (2004) 140–150.